AD-A274 392

|||||||||||||

S DTIC
ELECTE
DEC 27 1993
A

Experimental Verification of Tomographic Reconstruction of

Turbulent Air Flow Structure Using Optical Wavefront Measurements

THESIS

Bryon L. Pedersen
Captain, USAF

AFIT/GEO/ENG/93D-01

93 12 22 142

93-31029

||||||||||||||||||

Experimental Verification of Tomographic Reconstruction

of Turbulent Air Flow Structure

Using Optical Wave Front Sensor Measurements

THESIS

Presented to the Faculty of the Graduate School of Engineering

of the Air Force Institute of Technology

Air Education and Training Command

in Partial Fulfillment of the

Requirements for the Degree of

Master of Science in Electrical Engineering

Bryon L. Pedersen, B.S.

Captain, USAF

December 1993

DTIC QUALITY INSPECTED 5

Accesion For		
NTIS CRA&I		☑
DTIC TAB		☐
Unannounced		☐
Justification		
By		
Distribution /		
Availability Codes		
Dist	Avail and / or Special	
A-1		

Acknowledgements

I would like to take this opportunity to thank several people who helped bring this research to a successful conclusion. I would first like to thank my advisor, Dr Byron Welsh for his guidance and encouragement throughout the research. Captain Robert Johnson deserves my thanks for teaching my how to use the software required to analyze and present the data, and for answering a hundred computer related questions. Foremost, I would like to thank my wife Nancy and son Alex for standing by me through the course of this research. Their continuing support and encouragement made the long hours of work more bearable.

Table of Contents

List of Figures

Abstract

The performance of an aircraft based optical system is degraded by aero-optic turbulence. The varying index of refraction within the turbulent field causes phase perturbation in an optical wave. In order to compensate for aero-optic turbulence effects the nature of the turbulence must be understood. Large scale, organized structure within the turbulence has been found to contribute significantly to the overall phase perturbation caused by a turbulent field.

A unique approach was devised to determine the turbulence structure using tomographic reconstruction techniques. Tomography is a well developed science which provides cross-sectional information on an object. Tomography provides an excellent means to determine the underlying structure within a turbulent field. The phase perturbation of an optical wave passed through a turbulent field provides projection data for the tomographic reconstruction. The tomographic reconstruction results in a three-dimensional index of refraction plot of the turbulent field. This plot reveals the structure within the turbulent field.

An experiment was designed to determine the feasibility of the tomographic technique for reconstructing turbulence structure. A nozzle system was built to generate a turbulent field made up of jets of warm air. An optical wave was propagated through the turbulence and the induced phase perturbation was measured. A shearing interferometer was used to measure the wave front of the perturbed optical wave. The wave front phase map provided the projection data for a tomographic reconstruction of the index of refraction of the turbulent field.

Experimental Verification of Tomographic Reconstruction
of Turbulent Air Flow Structure
Using Optical Wave Front Sensor Measurements

I. Introduction

An optical wave propagating through the atmosphere is distorted by turbulence. All optical systems involving atmospheric transmission experience a degradation in performance due to the effects of turbulence. Systems such as communication or weapons systems experience a reduction in the power delivered by the optical wave. The problems created by turbulence are increased for an aircraft-based optical system because of the aero-optic effects [7]. Not only does the optical wave encounter atmospheric turbulence, it also must pass through the turbulent boundary layer which surrounds an aircraft in flight. The turbulence encountered in the aircraft boundary layer is referred to as aero-optic turbulence.

In order to enhance the performance of optical systems, it is necessary to correct or compensate for the perturbation caused by turbulence. It is necessary to understand the nature of turbulence, and how turbulence affects an optical wave before any compensation can be achieved.

Turbulence is a result of variation in temperature and pressure in the atmosphere. This variance in temperature and pressure leads to a varying index of refraction. Areas of constant index of refraction are referred to as eddies. Turbulence consists of eddies of varying size and varying index of refraction. Eddies generally start out at a large size and then are broken up by winds and mixing effects to smaller

1

and smaller sizes until they finally dissipate.

Both atmospheric turbulence and aero-optic turbulence consist of eddies, but the spatial and temporal properties of the two types of turbulence differ. Atmospheric turbulence tends to be of relatively large spatial scale, with eddies ranging in size from approximately 100 meters down to a few millimeters. Atmospheric turbulence also has relatively long term temporal characteristics. Aero-optic turbulence is of a much smaller spatial scale: eddies are on the order of a few millimeters or smaller, and fluctuate very rapidly.

A wave front transmitted through the atmosphere will encounter the fluctuating index of refraction and experience distortion. A great deal of work has gone into the study of atmospheric turbulence, in support of imaging systems. This work has led to techniques which allow for partial compensation of the degradation due to atmospheric transmission. It has been found that nearly all of the degradation caused by turbulence is in the form of phase aberration. The long term temporal character of atmospheric turbulence allows adaptive optics to provide phase compensation to a wave front to cancel out the effects of atmospheric turbulence. Current adaptive optics systems are not capable of operating at the speeds necessary to compensate for aero-optic turbulence. Further study is required to understand the nature of aero-optic turbulence which will lead to possible compensation techniques.

Aero-optical effects are generally studied by observing mixing layers and turbulent shear flows, generally referred to as turbulent flows. Early studies of turbulent flows used a statistical approach, and assumed that the turbulent flow was homogeneous [2,8]. This approach provided a statistical model of turbulent flows, but

2

provided little insight into the actual nature of the turbulence.

It is known that within the random eddies of a turbulent flow there exists large-scale organized structure. Recent studies of turbulent flows have focused on the large-scale organized structure and the structure's impact on the overall phase perturbation of an optical wave front [9,10,11]. These studies have revealed that the structure existing in the turbulent flow plays a significant role in the phase distortion of an optical wave front. Truman demonstrated that "in the near-wall region of a turbulent channel flow", large-scale structures occupied approximately 30 percent of the turbulent area but accounted for about 60 percent of the total phase error induced in a wave front [9]. The significance of the organized structure in the phase perturbation reveals the fact that the early assumptions of homogeneity were erroneous, and a turbulent flow is actually inhomogeneous or anisotropic in nature.

As stated earlier, current adaptive optics systems do not operate at sufficient speeds to provide phase compensation for boundary layer turbulence. However, the significance of the organized structure in a turbulent flow lends itself to a possible solution to provide a certain degree of phase compensation using current adaptive optics techniques. If the organized structure which exists within the aero-optic turbulence could be characterized or modeled, the phase perturbation caused by the structure could be compensated for. The use of adaptive optics requires the assumption that the organized structure is roughly constant for the response time of the adaptive optics systems, or that the time average of the structure is fairly constant.

The key to developing a compensation method using adaptive optics, or any other technique, is to obtain a better understanding of the nature of aero-optic

turbulence. Keeping in mind the anisotropic nature of a turbulent flow, three-dimensional modelling of a turbulent flow would provide the most thorough means of studying the turbulence. An established method for providing three dimensional modeling of a medium is tomography. (The basic theory of tomography will be presented in Section II.)

A unique approach to studying a turbulent flow has been devised which uses interferometric data in conjunction with tomography to provide three-dimensional measurements of a turbulent flow. An optical wave will be transmitted through a turbulent flow which has some known structure. A shearing interferometer will be used to obtain phase maps of the optical wave front distorted by the turbulent flow. The phase perturbation data will be fed into a tomographic reconstruction program to provide a three-dimensional image of the turbulent flow. Section III will provide a full description of the experimental procedure.

The variation in the index of refraction produces the phase perturbation which serves as the projection data for the tomographic reconstruction. Therefore, the image that is provide by the tomographic reconstruction program is actually a three-dimensional index of refraction plot of the turbulence. Similarly, the absorption data used for a CAT scan is produced by the density of the object, and the image provided by the tomographic reconstruction is a three-dimensional density plot of the object.

1.1 Scope

The overall goal of the present line of research is to develop a method of using wave front measurement and tomography to model aero-optic turbulence. The three-dimensional model of the turbulence provided by tomographic techniques would provide insight into the nature of the turbulence and lead to possible compensation methods for the wave front distortion caused by the turbulence.

The scope of the present effort is to experimentally verify the feasibility of using interferometric wave front measurements in conjunction with tomographic reconstruction to reconstruct an index of refraction plot of a turbulent flow. A turbulent flow with some known structure will be placed in the path of a laser beam. The resulting wave front phase of the laser beam will be measured using a shearing interferometer. The wave front phase measurement will be repeated for several viewing angles through the turbulent flow. The wave front phase data will then be fed into a tomographic reconstruction program to provide a plot of the index of refraction of the turbulent flow. The quality of the reconstructed image will then be examined to comment on the feasibility of the technique.

Section II provides an overview of the theory behind tomography, and how it will be applied to the current problem. Section III will describe the equipment and experimental setup to be used. The experimental procedure will be discussed in detail. Section IV will present the results of the experimentation and comment on the success of the measurement technique.

II. Background

The following section will provide a brief overview of the concept of tomographic reconstruction. The overview will cover the theory of tomography, the procedures involved in the use of tomography, and a short discussion on reconstruction techniques. The use of tomography in characterizing turbulence will then be discussed.

2.1 Tomography [1,3]

Tomography is an established technique for obtaining a three-dimensional image of an object. Tomography provides structural information about an object, including cross-sectional information about the interior of the object. One of the most useful aspects of tomography is the ability to obtain cross-sectional information on an object in a non-intrusive manner.

Tomography was originally developed primarily in the medical field as a method of providing cross-sectional images of the body. Computer aided tomography, or CAT scans, have been used for years to image the body, assisting in the location of abnormalities such as tumors. Recently, tomography has been finding increased applications in industry and many fields of science as a non-destructive means of obtaining high resolution three dimensional images of an object.

The data gathering procedure for tomography involves recording projection data from many different angular views through an object. The data from any given

6

angular view is referred to as a projection, and denoted by $p_\gamma(r)$. The set of all

projections is referred to as the projection data, and denoted by $p(r,\gamma)$. A projection is

obtained by illuminating the object of interest with an electromagnetic wave and

measuring some characteristic of the transmitted wave. In the case of a CAT scan, x-

rays are used to illuminate the object of interest. The magnitude of the transmitted

wave is measured. The projection, which represents the absorption of energy by the

object, is calculated from the measured data. The process is then repeated for many

angles through the object. Figure 1 illustrates the procedure for obtaining a projection

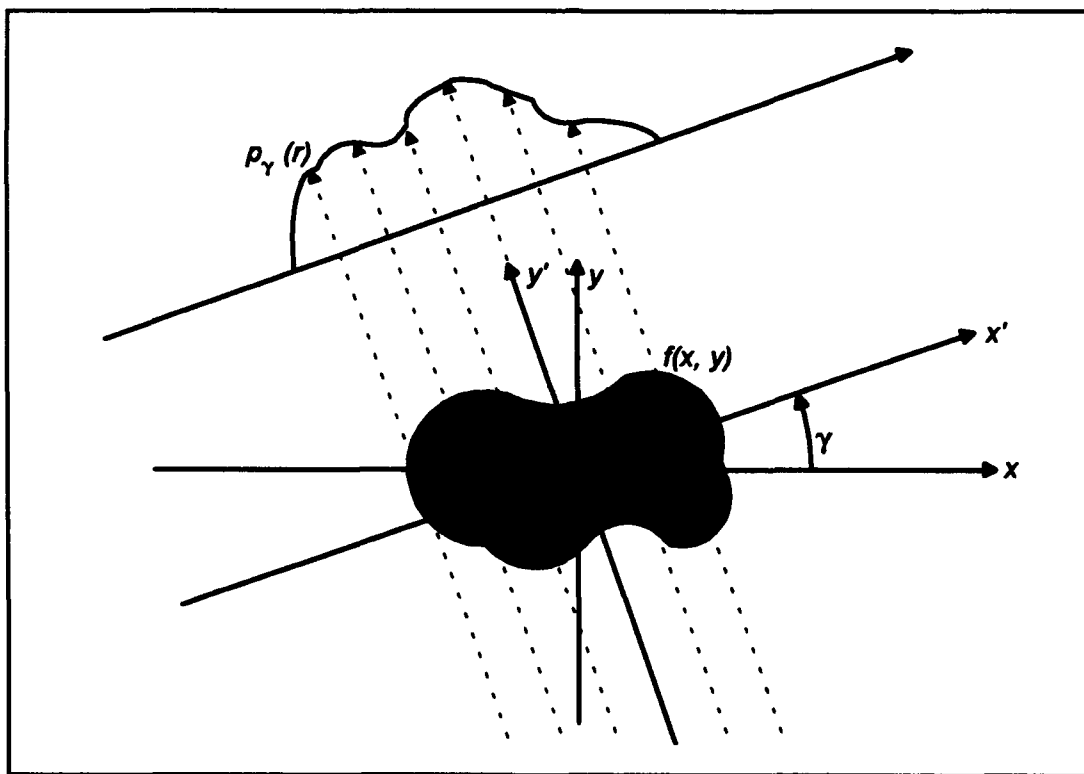from a two-dimensional object.

Figure 1. Projection through an object at angle γ.

The greater the number of projections obtained, the more complete the object

information will be and the reconstructed image will be more accurate. In 1917,

Radon proved that a complete set (infinite set) of noiseless projections from an object enable perfect reconstruction of the object . The limitation of the real world provide noisy projections taken at discrete, and generally evenly spaced intervals about the object. Projections are only needed over a 180 degree range of viewing angles because of symmetry.

Once a full set of projections has been recorded, a reconstruction algorithm is used to produce an image of the object. A multitude of reconstruction algorithms have been developed. The algorithms are variations of one of three general methods of reconstruction: algebraic reconstruction techniques (ART), convolutional-backprojection (CBP) techniques, and direct Fourier (DF) techniques [3]. The different techniques and the numerous variations provide varying degrees of success for any particular situation.

The most commonly implemented reconstruction technique is the CBP technique. The CBP technique, as well as the DF technique, is based on the projection slice theorem (PST), also referred to as the central slice theorem [1,3]. The PST describes the mathematical relationship between the projection data and the image. A proof of the PST will be presented to illustrate the principle behind the CBP and DF techniques. The development of the proof will follow that presented by Hayner and Jenkins [3]. The equations given by Hayner are for a two-dimensional object, but the mathematics can easily be extended to three dimensions.

Let the object be represented by $f(x, y)$, and the two-dimensional Fourier transform (2D-FT) of the object by $F(u, v)$. The projection at an angle γ is $p_\gamma(x')$, and the one-dimensional Fourier transform (1D-FT) of the projection is $P_\gamma(u')$. The x',

8

y' coordinate system represents the original x, y coordinate system rotated by the angle γ, and likewise, the u', v' coordinate system represents the rotated u, v Fourier coordinates. Mathematically, this rotation is represented by:

$$x = x'\cos\gamma \qquad y = y'\sin\gamma$$
$$u = u'\cos\gamma \qquad v = v'\sin\gamma \qquad (1)$$

Given these definitions, the PST states that $P_\gamma(u')$ equals the center cross-section slice of F(u, v) at the angle γ:

$$P_\gamma(u') = F(u'\cos\gamma, v'\sin\gamma) \qquad (2)$$

To prove this statement, start with the definition of the projection at an angle γ:

$$P_\gamma(x') = \int_{-\infty}^{\infty} f(x', y') \, dy' \qquad (3)$$

By the definition of the Fourier transform

$$P_\gamma(u') = \int_{-\infty}^{\infty} P_\gamma(x') \, e^{-ju'x'} \, dx' \qquad (4)$$

and

$$F(u', v') = \int_{-\infty}^{\infty}\int_{-\infty}^{\infty} f(x', y') \, e^{-j(u'x' + v'y')} \, dx' \, dy' \qquad (5)$$

Substituting (3) into (4) gives the equation:

$$P_\gamma(u') = \int_{-\infty}^{\infty}\int_{-\infty}^{\infty} f(x', y') \, e^{-ju'x'} \, dx' \, dy' \qquad (6)$$

Now consider the center cross-section slice of F(u, v) at the angle γ. This slice is defined as F(u', v'), where v' = 0. This definition allows us to equate (5) and (6)

$$\int_{-\infty}^{\infty}\int_{-\infty}^{\infty} f(x',y') e^{-ju'x'} dx' dy' = \int_{-\infty}^{\infty}\int_{-\infty}^{\infty} f(x',y') e^{-j(u'x'+v'y')} dx' dy' \Big|_{v'=0} \tag{7}$$

$$P_\gamma(u') = F(u',v') \Big|_{v'=0}$$

The equality in equation 7 proves the PST.

The concept of the center cross-section slice of F(u',v') discussed in the development of the PST can be illustrated by looking at an example of the transform relationship. A 1D-FT is performed on a complete set of projection data, $p(r, \gamma)$, to obtain $P(u', \gamma)$. $P(u', \gamma)$ describes the Fourier transform of the object, F(u,v), as shown by the PST. However, because of the discrete nature of the projection data, $P(u', \gamma)$ is only defined for discrete values of u' and γ. Therefore, F(u,v) is only defined at these discrete points on a polar raster as shown in Figure 2 [3]. The radial lines at a given angle γ illustrate the center cross-section slices of F(u,v) at that angle.

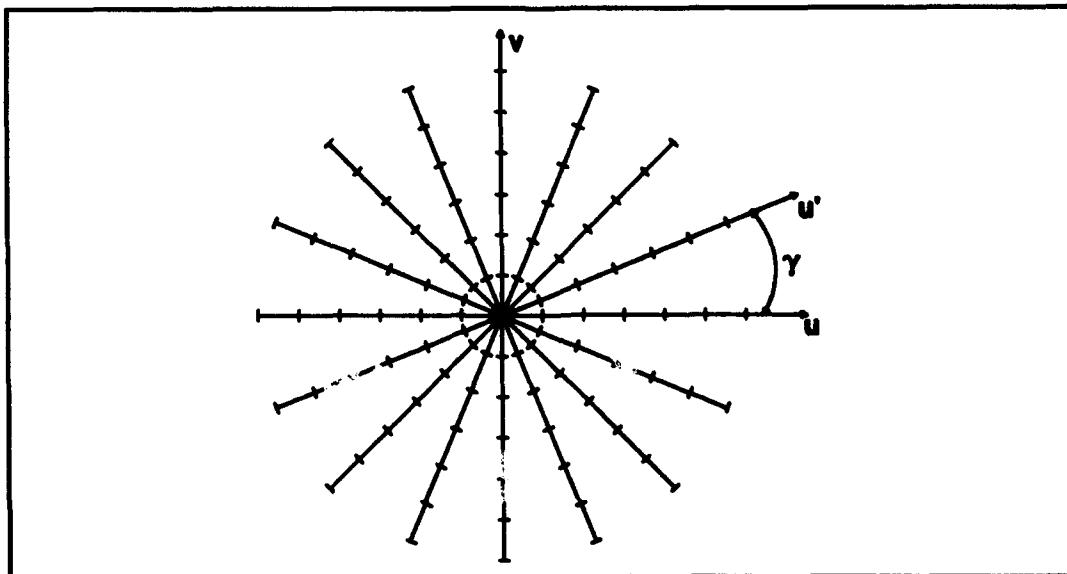The discrete nature of the samples and the resulting discrete nature of the

Figure 2. Discrete Fourier samples on a polar raster.

Fourier transform allows for only an approximation of the true image of the object. The approximation is further distorted by noise in the system. This is the reason why the PST is not implemented directly to reconstruct an image. The various reconstruction techniques have been developed to compensate for the distortions resulting from the discrete nature of the projection data and the noise of the system. Fully developed and verified reconstruction algorithms are available from various sources. A library of algorithms was obtained from Lawrence Berkeley Laboratory [4]. The Iterative Conjugate Gradient Method [4] was chosen for use in the current research. Capt. Robert Johnson, in a parallel research project, obtained the Lawrence Berkeley library and generated the computer program to utilize the chosen reconstruction algorithm. A detailed description of the reconstruction algorithm can be found in Capt. Johnson's thesis [5].

2.2 Tomography for Sensing Turbulence

As stated in the introduction, turbulence has an adverse effect on the propagation of and optical wave, causing phase perturbation of the wave front. Atmospheric turbulence has been well characterized, and techniques exist to compensate for the phase aberrations caused by atmospheric turbulence. Aero-optic turbulence has not been characterized to the same degree as atmospheric turbulence. The nature of aero-optic turbulence is difficult to model because of the small spatial scales and rapidly varying temporal character involved. Early studies of the effects of aero-optic turbulence, or turbulent flows, used a statistical approach, and assumed that

11

the turbulent flow was homogeneous [2, 8]. However, studies of turbulent flows indicated the presence of large-scale, organized structure within the flow. This indicated that the assumption of a homogeneous, isotropic flow was incorrect, and the statistical models could not account for the effects of the organized structure. Recent studies of aero-optic turbulence have focused on the effects of the organized structure [9, 10, 11]. It has been shown that the organized structure accounts for a significant portion of the overall phase perturbation caused by the turbulent flow. It is easier to characterize the organized structure within the turbulent flow because of the larger spatial scale and longer temporal character involved.

The problem now presented is the optimum way to understand the organized structure. Tomography, by its very nature, suggests an excellent, non-intrusive method to provide an understanding of the structure within a turbulent flow. The use of tomography requires the collection of projection data from the turbulence. The laser beam or optical wave, serves to illuminate the turbulence. The characteristic of the optical wave to be measured for use as projection data must be determined. To identify a parameter which will be useful, return to the definition of projection data. A projection is described by a line integral through the object, as shown by Equation 3. A characteristic of the optical wave which varies when integrated along the optical path through the turbulence is required to provide useful projection data. Since turbulence is a non-absorbing medium, absorption measurements, as used by CAT scanners, would be useless as projection data for this application.

The phase perturbation of the wave front caused by the turbulence provides exactly the type of information needed for projection data. The phase of the optical

wave is distorted by the varying index of refraction as it is integrated along the optical path through the turbulence, resulting in a distorted wave front. An optical wave with a known wave front is transmitted through a turbulent flow, and the resulting wave front measured. The phase distortion of the wave front is measured, providing a projection. The optical wave is transmitted through the turbulent flow at various angles to provide a set of projection data. Tomographic reconstruction results in a three-dimensional (3D) image of the turbulent flow, or more precisely, a 3D plot of the index of refraction of the turbulent flow. The model of the turbulent flow could then be used to calculate the phase perturbation which would result for any propagation path through the flow.

The limiting factor in the tomographic modeling of the turbulent flow is the time frame involved in gathering the projection data and the tomographic reconstruction. For the technique to be useful, the organized structure must have a relatively constant time average over the interval required for the tomographic process. The index of refraction variations from the small scale random eddies would average to near zero over the time average, and the majority of the reconstructed model would result from the organized structure. As stated earlier the organized structure contributes significantly to the overall phase distortion, therefore, it is reasonable to assume that a time averaged view will provide significant information on the phase effects which can be expected from a turbulent flow.

III. Experimental Setup and Procedures

A unique experiment to characterize turbulence through the use of tomography has been developed. A shearing interferometer will be used to measure the phase perturbation induced in an optical wave by a turbulent field with some known structure. The phase perturbation will be measured at various angles to provide the projection data for a tomographic reconstruction of the turbulent field. The reconstruction will provide a three-dimensional plot of the index of refraction of the turbulent field, and reveal the structure present in the turbulence.

A description of the experimental equipment, the setup, and the experimental procedure used to acquire the projection data will be discussed in this chapter. The shearing interferometer and the supporting software will be discussed in Section 3.1. Section 3.2 will describe the nozzle used to produce the turbulence. The experimental setup will be outlined in Section 3.3. Finally, the experimental procedure followed to collect the projection data will be detailed in Section 3.4.

3.1 Shearing interferometer

The projection data desired for the experiment requires measurement of the wavefront of an optical wave. A shearing interferometer is used to obtain these measurements. A shearing interferometer and associated software were available in the AFIT Adaptive and Atmospheric Optics Laboratory from a previous study of turbulence effects. A brief outline of the theory and operation of the interferometer

14

and software will be presented below. A more detailed description, including the mathematics behind the theory, can be found in the thesis of Magee [6].

Figure 3 shows the layout of the shearing interferometer (SI). The x and y legs of the SI are identical, so the following discussion of the operation of the SI applies to either leg. Once the input beam enters one leg of the interferometer, a polarizing beam splitter (PBS) and two mirrors are used to produce two parallel beams with a lateral shear between them. Figure 4 illustrates how this lateral shear is achieved by a slight rotation of the PBS. The sheared beams are recombined by the analyzers resulting in interference, or fringe patterns. The fringe patterns are recorded by the CCD cameras.
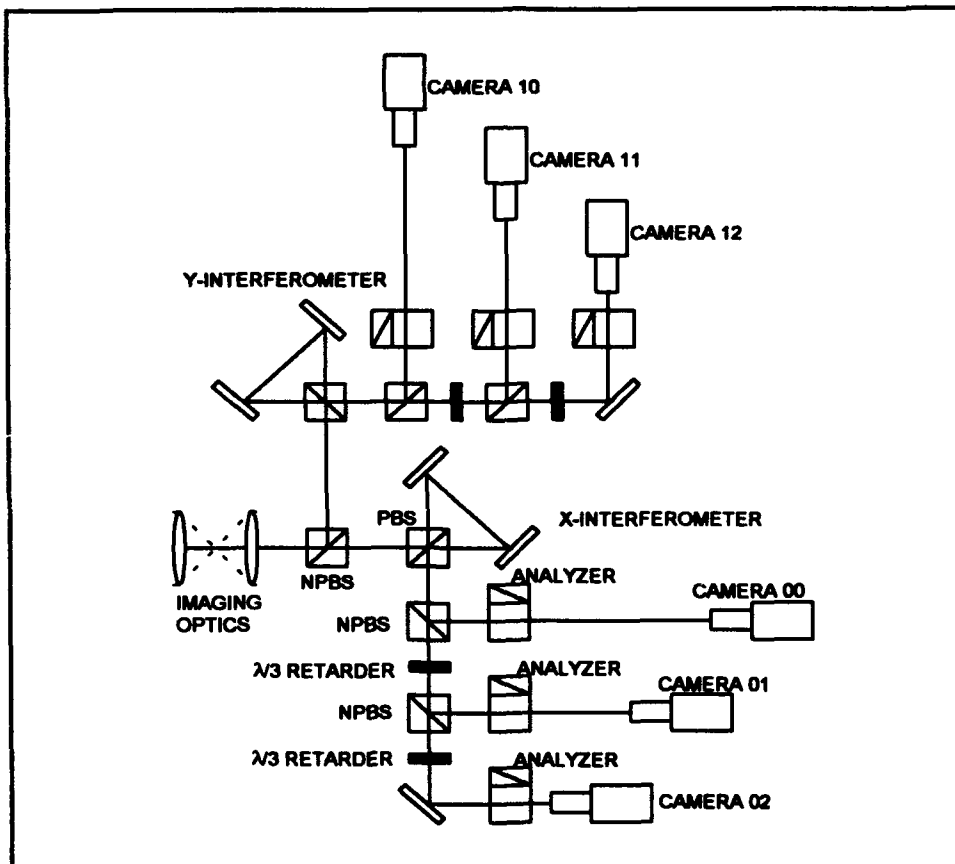
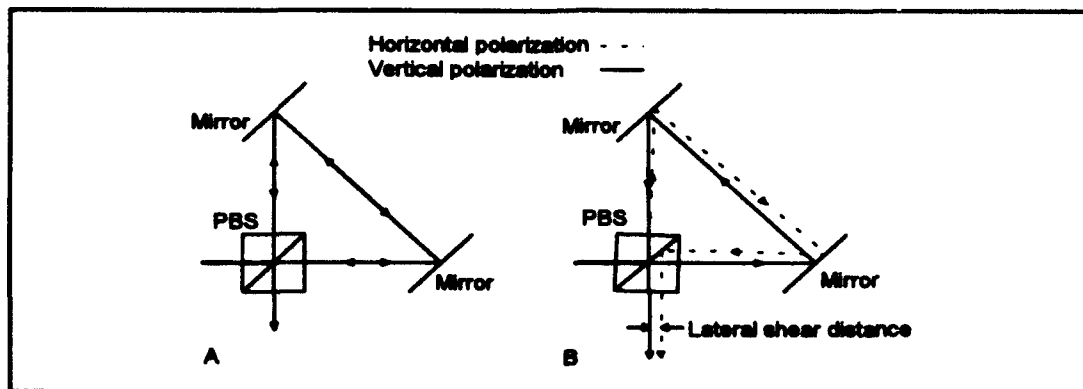**Figure 3.** Shearing interferometer (SI).

Figure 4. Producing lateral shear in the shearing interferometer. A.) No shear, B.)shear produced by a rotation of the PBS.

Three interference patterns are recorded by each leg of the SI. The sheared beams are divided among three different optical paths along the leg of the SI, one path to each of the three cameras. The optical path length is altered for each of the three separate paths by the introduction of $\lambda/3$ waveplates (see Figure 3). Each of the waveplates introduces a phase delay of 120 degrees to the sheared beams. The three, phase shifted interference patterns provide the data necessary for the software to calculate the wave front phase difference across each pixel in the display. To fully describe the wave front, the phase difference across each pixel must be found in both the x and y-directions. The two legs of the interferometer provide the data in both the x and y-directions. The input of the interferometer is designed in such a way that the lateral shear is induced in the x-direction in one leg of the SI, and in the orthogonal, or y-direction, in the other leg.

The software which provides the analysis of the interferometer data was supplied with the equipment. The code is written in Interactive Data Language (IDL), a language designed for image processing, and is hosted on a Sun-4 computer. Two Androx boards in the Sun-4 act as frame grabbers to provide the interface between the

SI output and the computer. The output from the six CCD cameras is displayed on six monitors, from which the Androx boards grab the images of the interference patterns. The interferometer software performs extensive computations on the data provided by the six interference patterns to arrive at a phase map of the wavefront. Examples of the phase map provided by the software are shown in Figures 5 and 6 on the following page.

3.2 Turbulence generator

A tremendous amount of thought was involved in determining how to produce the turbulence for this experiment. As stated in the introduction, the objective is to try to reconstruct the organized structure within turbulence. The difficulty in developing the turbulence was related to the fact that the turbulence must have a known structure. Without knowledge of the structure, no analysis of the success of the tomographic reconstruction would be possible. A nozzle emitting a jet of warm air was chosen as the source of turbulence. The time averaged structure of the jet air would be a jet, or tube, of air with a lower index of refraction than the ambient air. The design of the nozzle system was simple, but proved quite effective for the purposes of this experiment. A heat gun was directed into a funnel and the hot air was forced out a set of apertures in a faceplate to provide jets of warm air. The aperture of the nozzle was placed in the optical setup such that the jets of air traveled perpendicular to the path of the laser beam. Figure 7 shows the general setup of the nozzle system. The aperture of the nozzle consisted of a pattern of holes cut into a flat faceplate, or
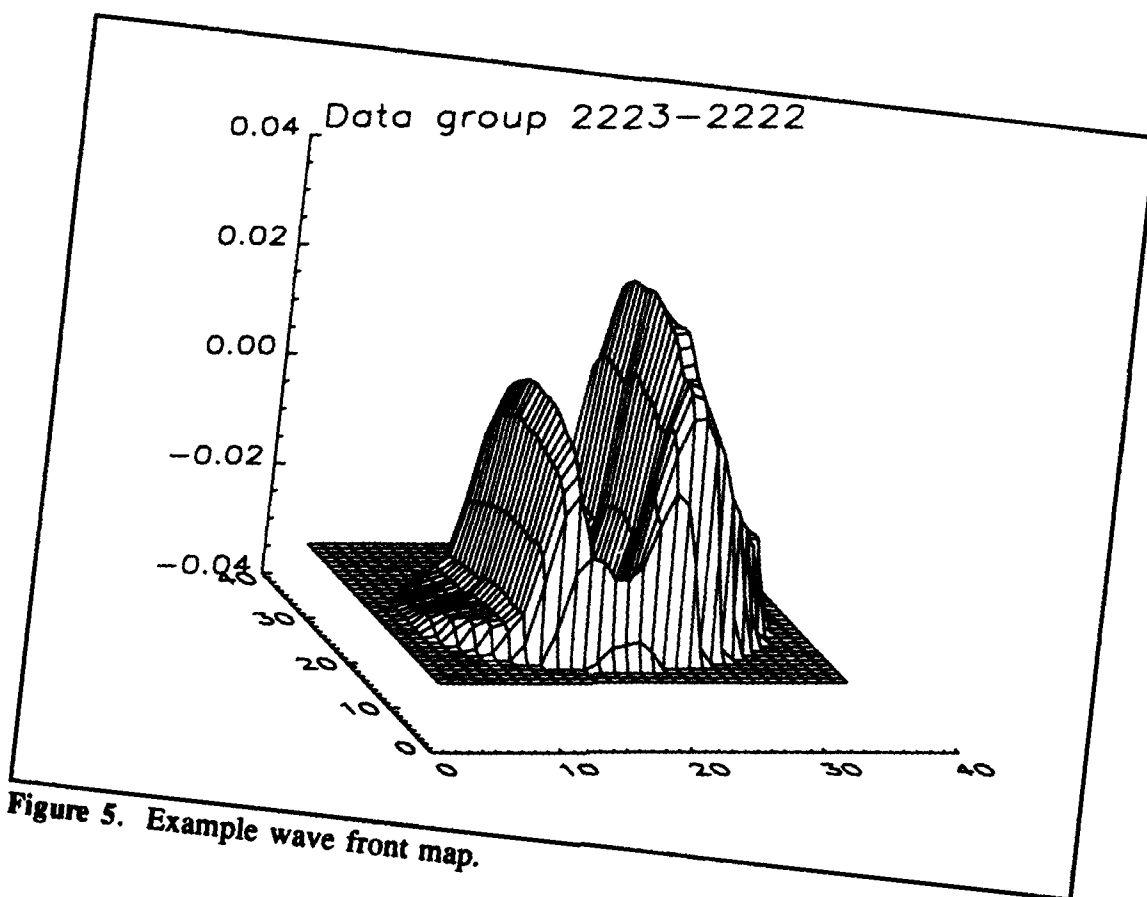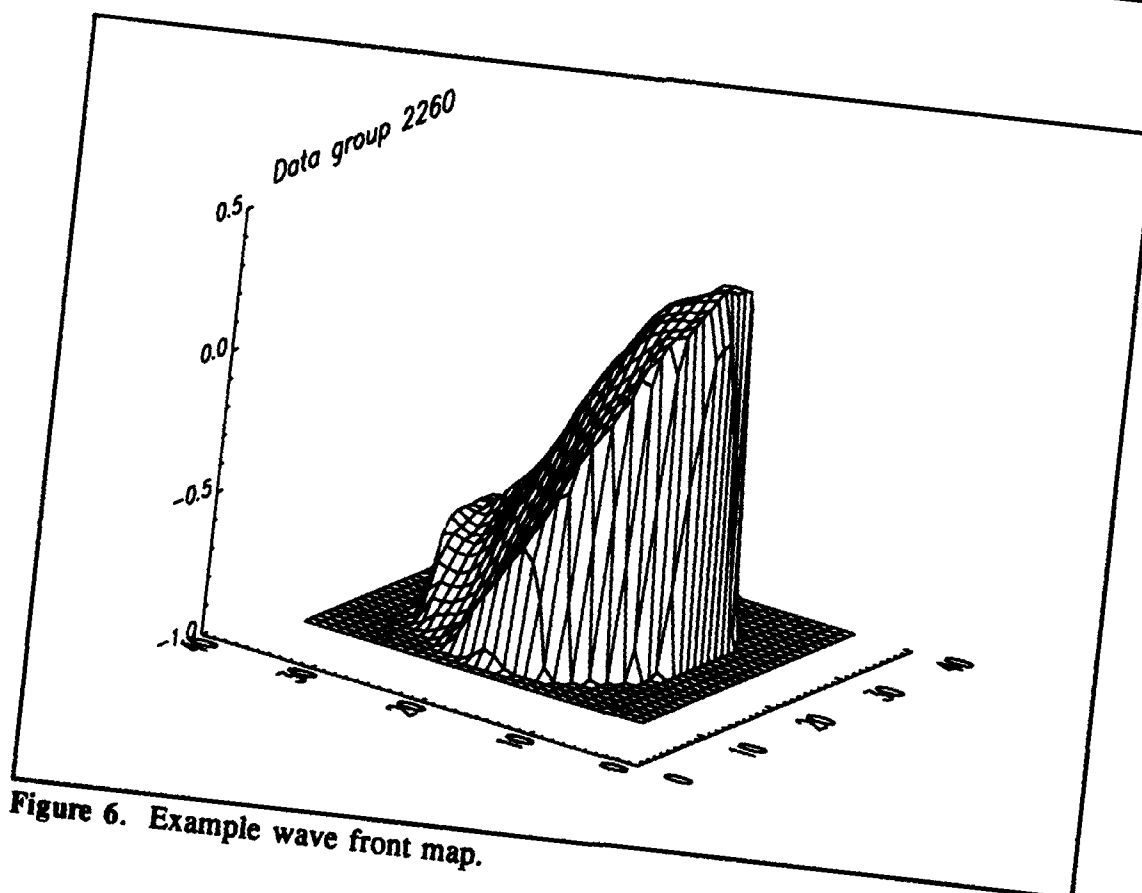
17

Figure 5. Example wave front map.

Figure 6. Example wave front map.

18

template. Figure 8 shows the three templates used in the experiment to create different turbulent fields, or different structure within the
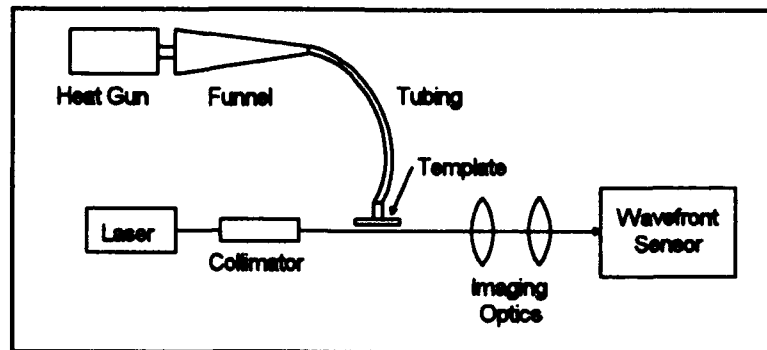

Figure 7. Turbulence generator and the location of the nozzle aperture in the experimental setup.

turbulent field. Multiple apertures in a single template were used to produce more structure, and asymmetric structure, within the turbulent field.
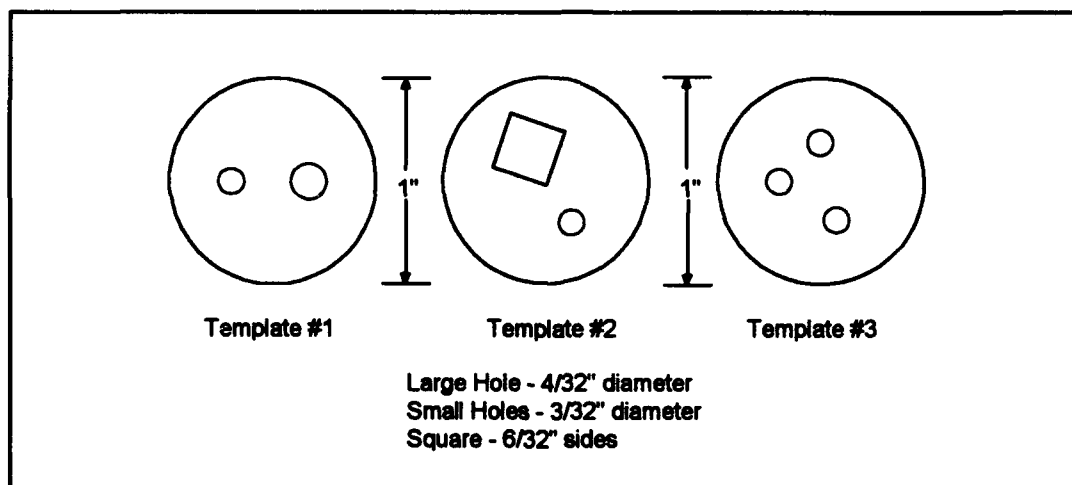

Figure 8. Nozzle aperture templates.

The nozzle system which produced the turbulence, radiated tremendous amounts of heat during the data gathering process. It was necessary to take precautions to prevent the radiated heat from interfering with the propagation of the laser anywhere other than at the nozzle aperture. The radiating heat from any part of the nozzle system could introduce additional phase perturbation in the wave front. The heat gun and funnel were placed off of the optical table to prevent any vibrational

or radiant heat induced perturbation in the optical system. A length of tubing was used to carry the hot air from the funnel to the location of the nozzle aperture on the optical table. The tubing was required to crossed the optical path to reach the proper location on the table. The heat radiating from the tubing would tend to rise and cause turbulence in the optical path. To prevent any phase perturbation resulting from the radiating heat, the tubing was elevated well above the optical path, allowing the heat to dissipate above the optical system.

The projection data needed for tomography must be obtained for multiple angular views through the object. The templates were placed in a rotational mount with angular markings to provide this angular flexibility. When the mount was rotated, the template was rotated about the center of the plate, as illustrated in Figure 9. Rotating the template caused the laser beam to passed through the turbulence at a different angle, providing a different projection angle.
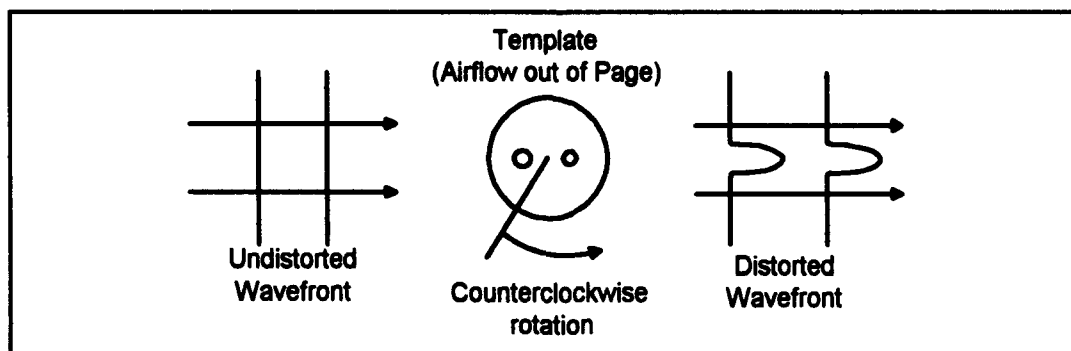

Figure 9. Rotation of nozzle template to vary projection angle.

The experimental setup used by Magee [6] was retained for use in the current experiment. The following section will trace the optical path as illustrated in Figure 10, and describe the components of the optical system.
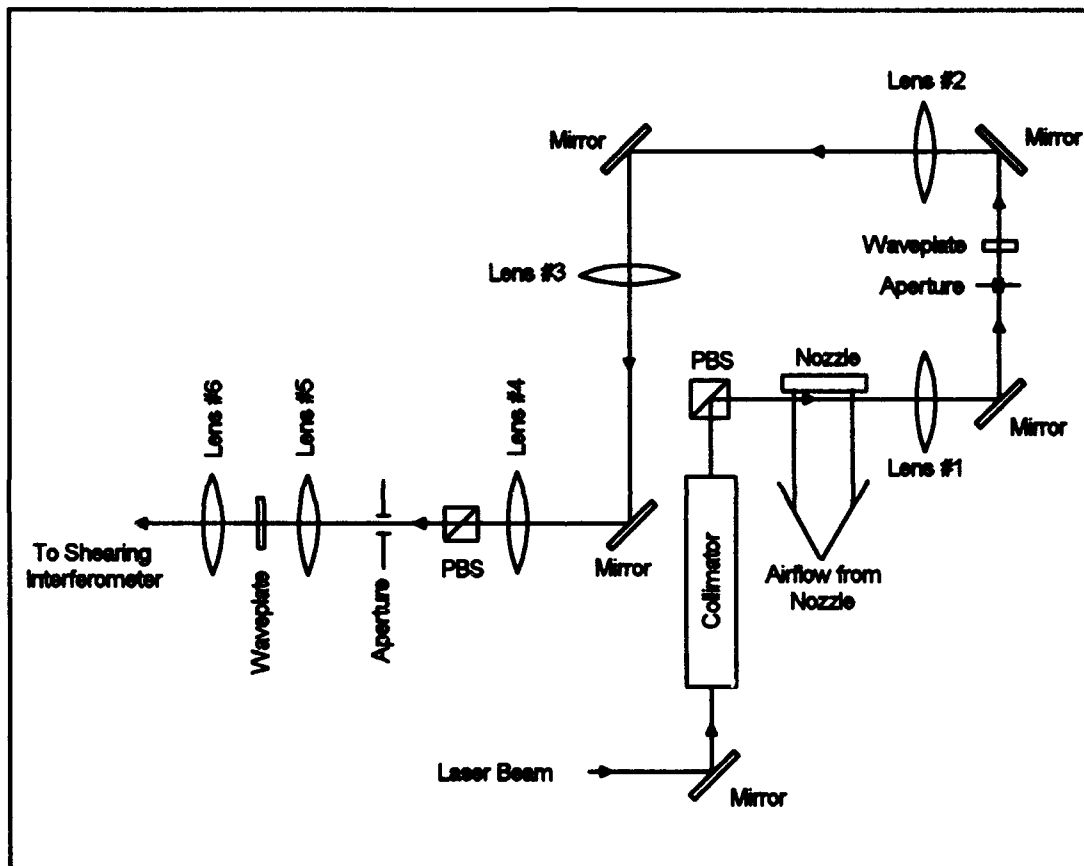

Figure 10. Experimental setup.

The laser beam is collimated and passed through a polarizing beam splitter (PBS). The beam of interest from the PBS is linearly polarized in the vertical direction. This vertically polarized beam is passed through the turbulence. Lenses 1 and 2 form a re-imaging system. The aperture between lenses 1 and 2 is set at the focal plane and used to filter out noise. The waveplate flips the polarization of the

beam to horizontal polarization. Lenses 3 and 4 form another re-imaging system, with a reduced image formed at the aperture. The aperture is a circular aperture, and is the input aperture for the shearing interferometer (SI). The PBS between lens 4 and the aperture passes only the horizontally polarized light. Lenses 5 and 6 also form a re-imaging system, imaging from the circular aperture to the input plane of the SI. The waveplate between lens 5 and lens 6 is an adjustable polarizer used to determine the polarization of the light to the SI. The polarizer is rotated to pass horizontal, vertical, or both polarizations.

3.4 Experimental procedure

The procedure for gathering a set of data for one of the nozzle templates is outlined in this section. The analysis required to obtain the projection data will also be discussed.

The laser was turned on and allowed to warm up for approximately 30 minutes to ensure that the laser output was stabilized. Before data could be gathered, the SI needed to be calibrated. The outline below describes the calibrations performed on the SI. The reason for the calibrations are discussed without the details of how the calibration is performed. Appendix B of the thesis by Magee [6] contains detailed instructions on the procedures involved in the various calibrations required . The calibration values, gain/offset and shear, are needed for the software to correctly analyze the data to obtain the wave front phase maps. The first calibration performed was the gain and offset calibration which "calculates the gain and offset adjustments

22

for the cameras based on the linear relationship between beam intensity and image intensity." [6] The calibration procedure determined the gain and offset necessary for each camera to have the same linear relationship between the two intensity values. Next, the alignment of the cameras was checked. This involved a physical alignment of the cameras, referenced to camera 00, to ensure that the camera images were aligned. The final calibration was a measurement of the shear. The shear is determined by placing a pinhole in the aperture plane, and acquiring an image for both horizontal and vertical polarization input to the SI. Referring to Figure 4, one of the sheared beams produced in each leg of the SI is vertically polarized and the other is horizontally polarized. If the input to the SI is a single polarization, sheared beams will not be produced. Only one beam, with the polarization of the input, will be propagated down the legs of the interferometer. It then follows that by measuring the offset of the centroid of the two pinhole images, one obtained for each polarization input to the SI, a measure of the shear is provided. Several data points are gathered both before and after the data acquisition and average to obtain the shear measurement used in the data analysis.

With the SI calibrated, the projection data was collected. A set of reference data was gathered first. The reference provides the phase of the wave front with no turbulence present in the optical path. Theoretically, the optical wave in the system with no turbulence should have a planar wave front. Due to slight misalignment of the optical components, particularly the re-imaging optics, and imperfections in the optics the wave front is not planar. Figure 5 is a typical reference wave front. The reference wave front is subtracted from the wave front obtained in the presence of the

turbulence. The resulting wavefront used for the projection data represents the phase perturbation caused by the turbulence only. Because of the time frame involved in the data acquisition new reference data was obtained periodically to ensure the accuracy of the reference wave front.

Projection data in this experiment was gathered at 19 different angles; zero to 180 degrees in ten degree increments. (Because of symmetry, the data at 180 degrees is identical to the data at zero degrees. The reconstruction algorithm used recognized this redundancy in data and ignored the data at 180 degrees). As pointed out in the Introduction, the information of interest is the organized structure of within the turbulence. For the jets of warm air created for this experiment, the structure will simply consist of jets of lower index of refraction. The structure can be reconstructed by obtaining time averaged phase perturbation data. At each projection angle, a total of eight data frames were gathered over a time frame of approximately one and a half minutes to determine the time averaged wavefront. The video system used two to one interlacing, so the data sets actually consisted of 16 sets of interference patterns. The set of 16 interference patterns at any one projection angle was referred to as a data group.

Early testing with the nozzle system showed that the heat gun could only be operated at the hot setting for approximately three minutes before the tubing started to smoke. In addition, if the tubing was left attached to the nozzle throughout the data acquisition, the nozzle became hot enough to introduce additional turbulence from heat dissipation. To compensate for these problems, the heat gun had to be turned to cool, and the tubing disconnected from the nozzle between data groups to allow the system

24

to cool.

The funnel and tubing system was heated before the data acquisition process. The procedure for acquisition of a single data group at any given angle required the tubing to be connected to the nozzle and the heat gun turned to hot. The system was run for 30 seconds to stabilize, and then the data group was acquired. The system required approximately one and one half minutes to acquire an entire data group. When the acquisition was complete the heat gun was turned to cool, and the tubing was disconnected from the nozzle. The system was allowed to cool for about three minutes prior to gathering the next data group. Approximately three hours were required to gather the complete data set for the 19 angular views.

Once all the data was acquired for all angular views, the data was analyzed. The analysis involved the calculations required to produce the phase maps of each wave front. The wave front phase was determined for each of the 16 sets of interference patterns within a data group, and an average phase was also determined for each group. The average phase represented the time averaged wavefront. The final step in the data analysis was to subtract the reference phase from the average phase (as discussed above). The subtraction of the reference phase provided the time averaged wave front. The wave front represents the time averaged phase perturbation induced on the optical wave by the turbulence, which is the projection data desired. A set of wave front maps, or the projection data, for template #3 (see Figure 8) is presented in the Appendix.

IV. Results

The projections provided by the shearing interferometer (SI) software are two-dimensional arrays of 128 by 128 data points. The circular aperture which is the input aperture of the SI (see Section 3.3 and Figure 10) is roughly centered within this array. The projection contains useful information only within the circular plane described by the aperture. The circular plane is evident in Figures 5 and 6, as well as the projection data in the Appendix. The reconstruction algorithm used only a 90 by 90 array taken from the center of the projections. This limited array was used to eliminate as much of the area outside the aperture as possible, since there is no data outside the aperture. The Iterative Conjugate Gradient algorithm was used to perform the reconstruction [4], using five iterations. Tests were done with additional iterations which showed no improvement, and even some degradation with larger numbers of iterations. The reconstruction algorithm was set up to reconstruct on a spherical volume, due to the circular projection data. The reconstruction algorithm produced a 90 by 90 by 90 three-dimensional (3-D) plot of the index of refraction for the turbulent field. The reconstructed plot was compared to the expected index of refraction to determine the success of the tomographic technique. We had no way to measure the actual value of the index of refraction in the turbulent field, so the comparison of the reconstruction is qualitative in nature rather than quantitative. The nature of the index of refraction variation caused by the nozzle is fairly well defined in the time average sense. As discussed in Section 3.2, the nozzle creates jets of warm air which have a lower index of refraction than the surrounding ambient air.

The index of refraction would be the lowest at the center of the jet, rising to the ambient level at the outer edge of the jet of air. The width of the jet of warm air would be expected to increase as it moved away from the nozzle. As the jet of air widens and the warm air begins to disperse, the maximum value of the index of refraction in the tube would increase toward the ambient value. Therefore, the reconstructed 3-D plot of the index of refraction should show jets, or tubes, of low index of refraction. The tubes should have the lowest value at the center, and there should be a widening of the tube at greater distances from the nozzle aperture.

The 3-D reconstructed plots of the index of refraction were viewed with the aid of the Interactive Data Language (IDL) *Slicer* application. The *Slicer* allows the display of one or multiple cross-sectional views through the 3-D plot of the index of refraction. The cross-sectional views can be in any one or a combination of three planes: the x-y plane, the x-z plane, or the y-z plane. The position of the plane can be adjusted to any point in the plot along the axis orthogonal to the plane. The cross-sections are plotted in a false color scheme by the IDL *Slicer*. The cross-sections were then converted to grayscale. The grayscale was inverted such that a darker color refers to a lower index of refraction. A routine was developed to provide a two-dimensional surface plot of the index of refraction value for any given cross-sectional view. The values on the surface plot are also inverted, i.e., a high value represents a low index of refraction. Therefore, the tubes of low index of refraction will be represented by peaks in the surface plot of a cross-section.

A discussion of the coordinate system of the optical system is needed to help relate the orientation of the projections and the reconstructed index of refraction plot.

The axes were determined by how the software defined the data received from the shearing interferometer. The x-axis is in the vertical direction, with positive x in the upward direction. The y-axis is in the direction of the air flow, with the positive y direction toward the nozzle. The z-axis is along the optical path, with the positive direction counter to the propagation direction. The axes must then be related to the 90 by 90 by 90 reconstructed plot. Figure 11 shows the position of the axes on the square in which the reconstructed index of refraction is plotted by the IDL *Slicer*.
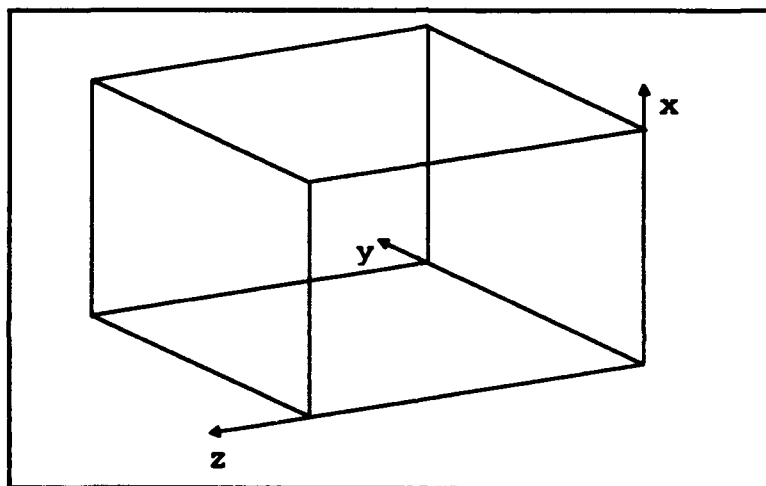
Figure 11. Coordinate system of the reconstruction.

4.1 Reconstruction for nozzle template #1

The reconstructed index of refraction plot turned out as expected for nozzle template #1. Figure 13 shows two cuts through the plot, one at y = 75 and the other at z = 21. The cross -sections clearly show the circular nature of the jets, with the lowest index of refraction in the center. The cross-section along the length of the jet indicates a slight widening of the jet. The plot also illustrates the increase of the index

28

of refraction as the distance from the nozzle aperture increases (see discussion above).

Figures 14 and 15 are surface maps of the cross-sectional planes shown in Figure 13.

Figure 14 is the surface map of the x-z plane at y = 75. Figure 15 is the surface map

of the x-y plane at z = 21. Figure 16 shows another cross-section at y = 15. Figure

16 further illustrates the widening and increase in index of refraction away from the

nozzle aperture. Figure 17 is the surface map of the cross-sectional plane shown in

Figure 16, the x-z plane at y = 15. The surface maps also illustrate the characteristics

of the reconstructed index of refraction as discussed above.

The only major aberration in the reconstructed plot of the index of refraction is

the presence of the crescent shaped notch in the outer edge of all of the reconstructed

jets. This aberration appears in the reconstructed plots for all of the templates. The

aberration is related to the circular aperture which defines the projection plane, as

described in the preceding section. The aperture tends to block the edges of the

projections. The amount blocked is different for each projection angle, as illustrated

in Figure 12. The square around the projections in Figure 12 represents the effect of

the aperture. As can
be seen, the aperture
blocks significantly
more data from
projection 2 than from
projection 1. As a
result of the aperture
the projection data is
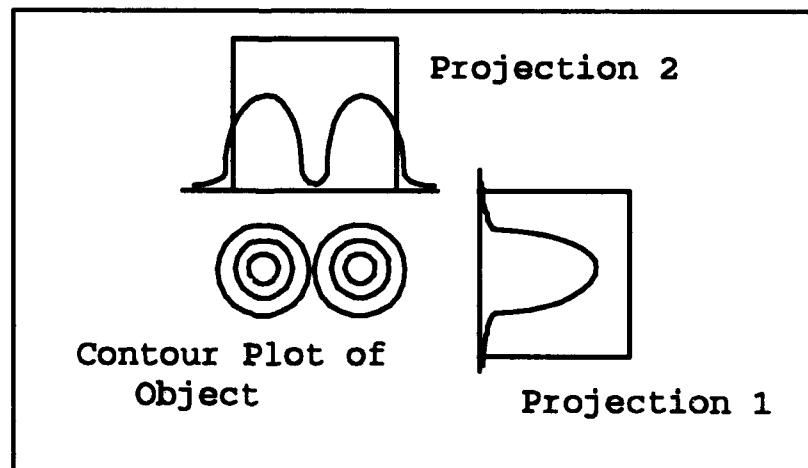
Figure 12. Effect of the aperture on the projection data.

not consistent near the edge of the aperture, due to the loss of different amounts of data from each projection. Therefore, the reconstruction is not accurate at the edges of the aperture. This is the reason the notch in the all the reconstructed jets appears on the side nearest the edge of the aperture. The loss of data resulting from the aperture can be noted in the projections shown in the Appendix. Note the immediate step of the phase inside the aperture. If no data was lost there would be no sharp transition of the phase at the aperture boundary.
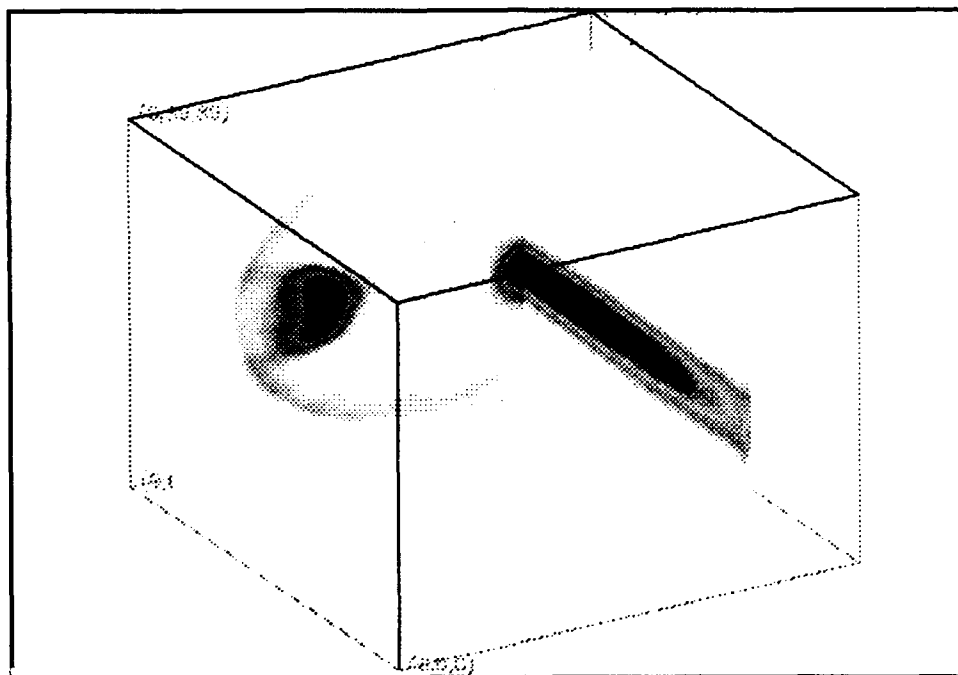
Figure 13. Cross-sections of the reconstructed index of refraction plot for template #1 at Y=75 and Z=21.
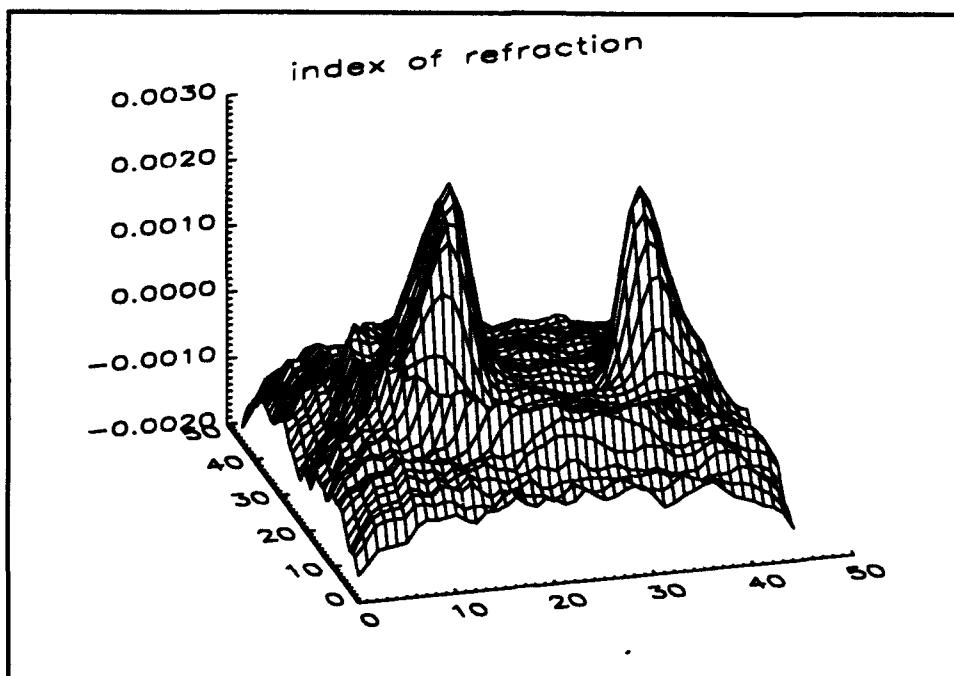
Figure 14. Plot of index of refraction variation, $2\pi\Delta n$, in the x-z plane at y=75, template #1.
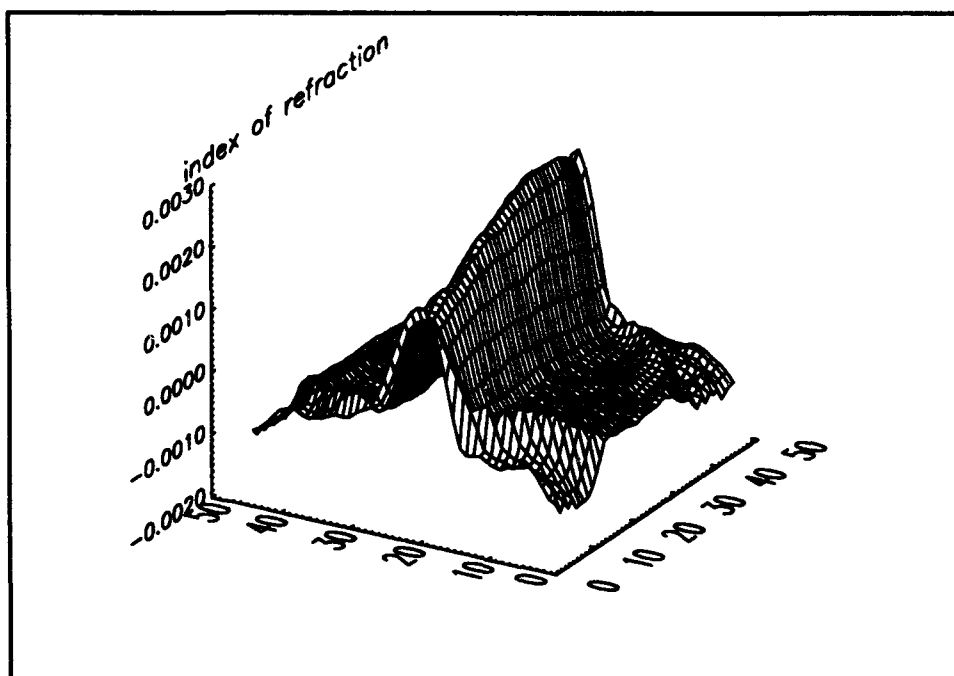
Figure 15. Plot of index of refraction variation, $2\pi\Delta n$, in the x-y plane at z=21, template #1.
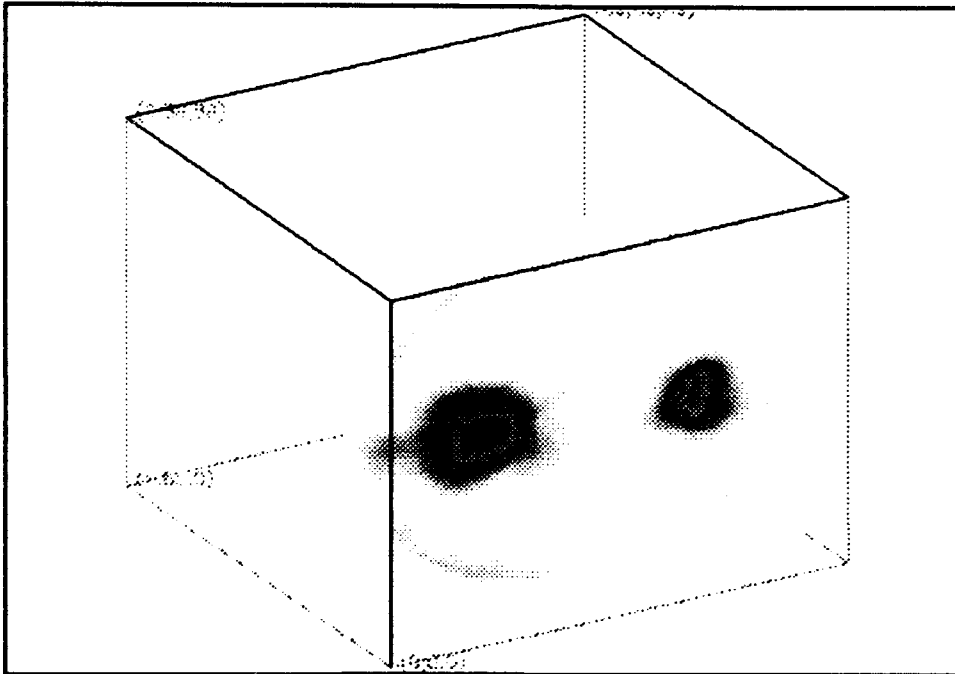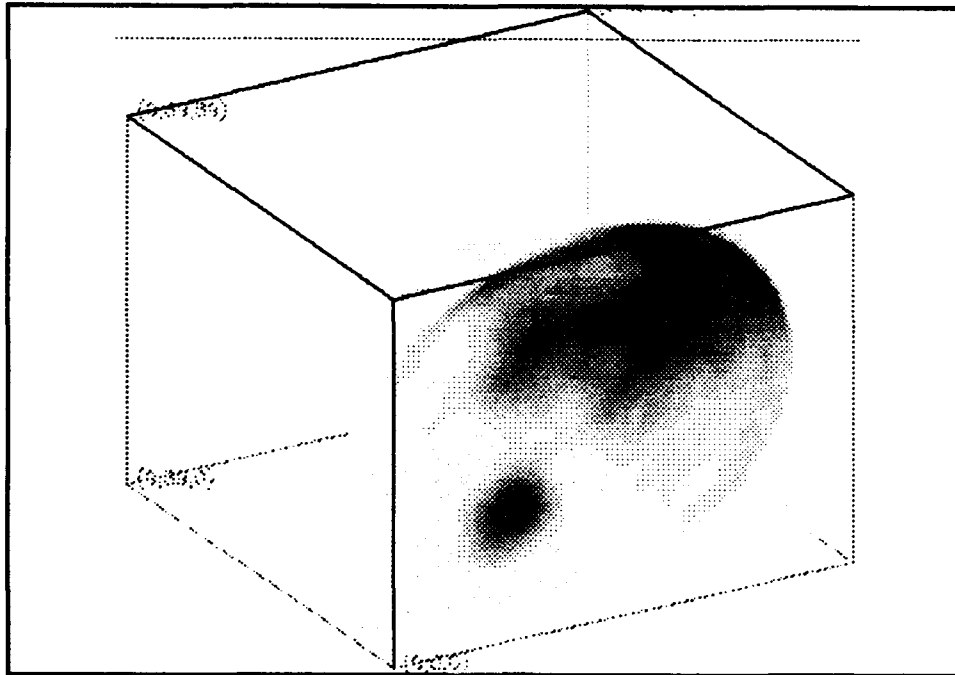
Figure 16. Cross-section of the reconstructed index of refraction plot for template #1 at Y=15.
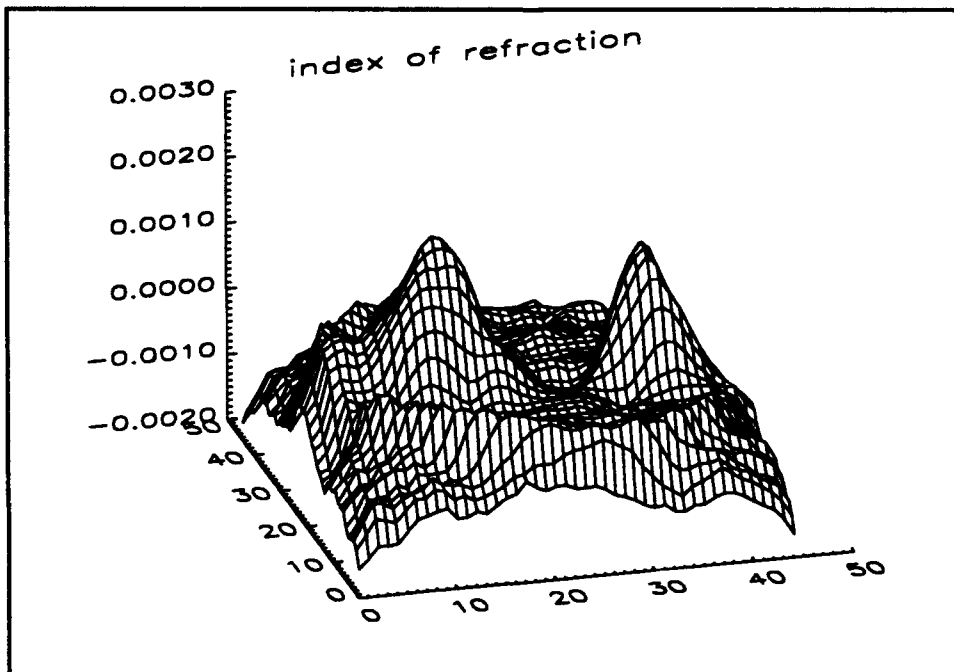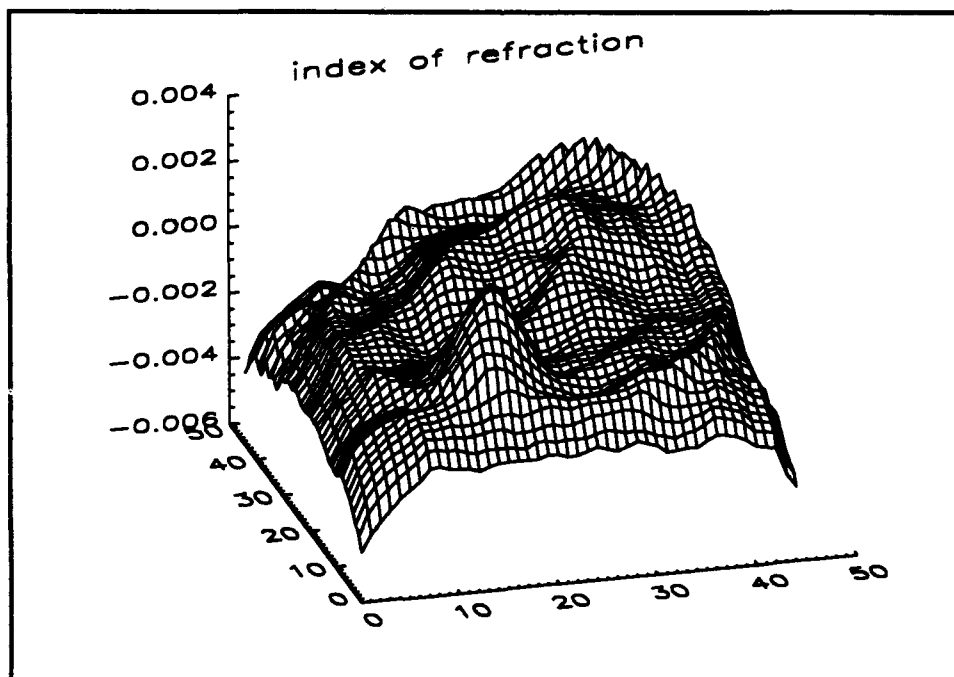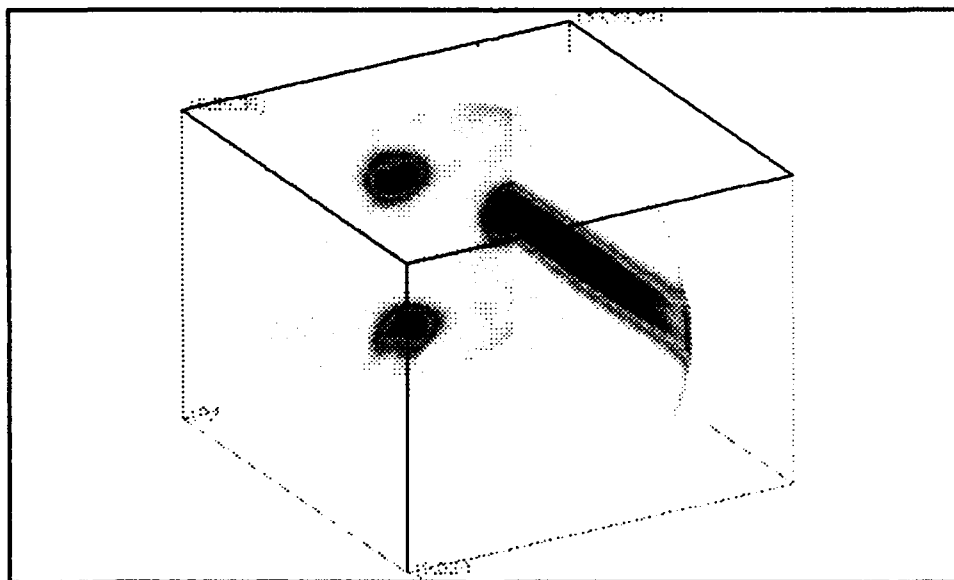

Figure 17. Plot of index of refraction variation, $2\pi\Delta n$, in the x-z plane at y=15, template #1.

The reconstructed plot for nozzle template #2 did not provide the same results as template #1. The square aperture was not a good test aperture. An air flow will not hold a square shape, but will quickly disperse toward a more rounded shape. The square hole was also quite large compared to the other apertures, so the air was flowing out at a slower speed. The slower speed would also contribute to a quicker dispersion of the air from the square aperture. The circular aperture did show all the expected characteristics. The index of refraction variations are small, since there was little air flowing out of the circular aperture due to the large size of the square aperture. Figure 18 shows the jets near the nozzle. Figures 19 and 20 show the surface plots for Figure 18. Figure 21 shows a cross-section farther from the nozzle, and Figure 22 is the surface plot for the cross-section in Figure 21.
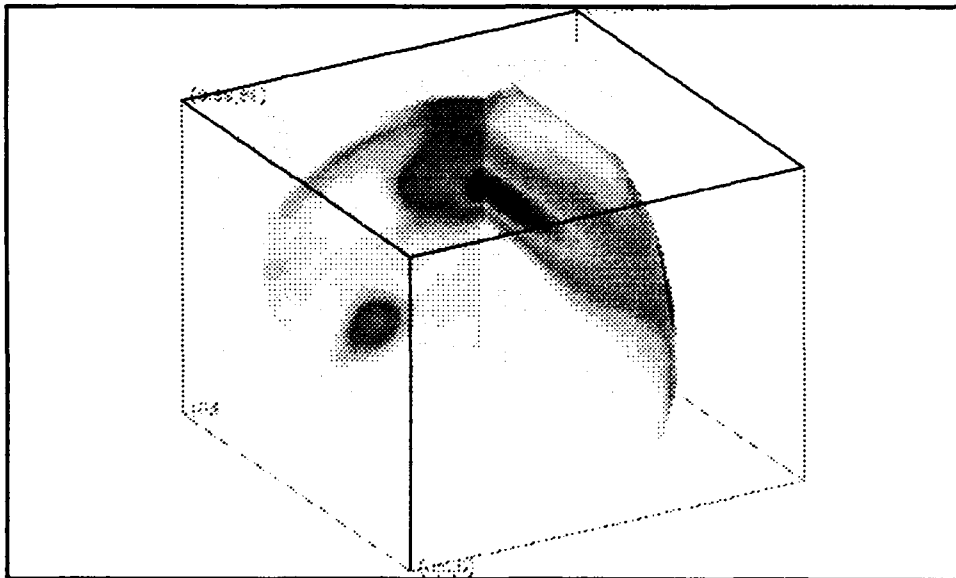
Figure 18. Cross-sections of the reconstructed index of refraction plot for template #2 at Y=75 and Z=29.
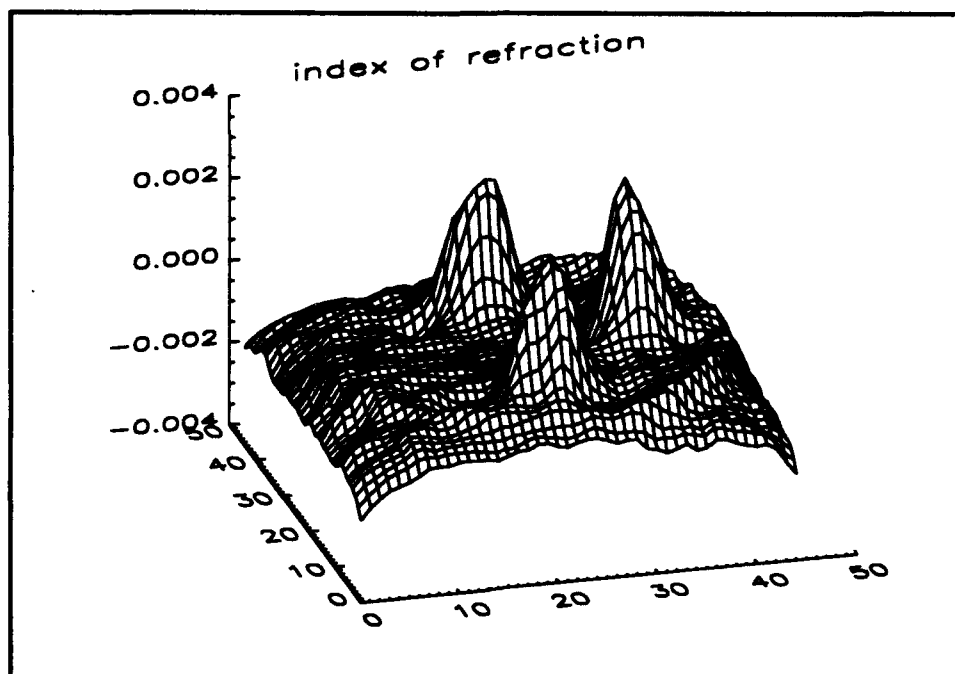
33
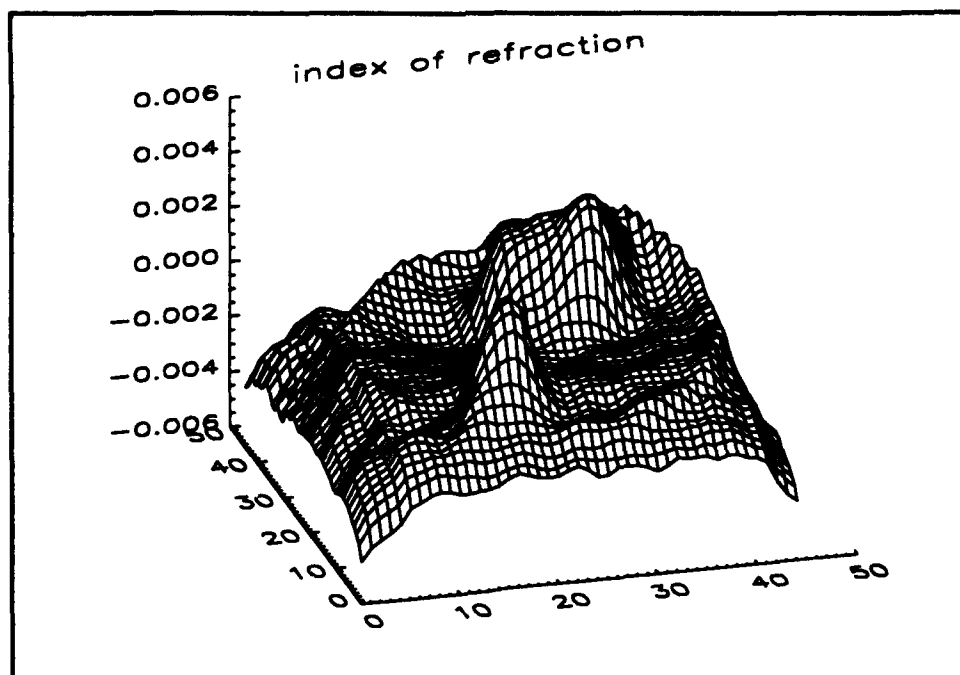
Figure 19. Plot of index of refraction variation, $2\pi\Delta n$, in the x-z plane at y=75, template #2.
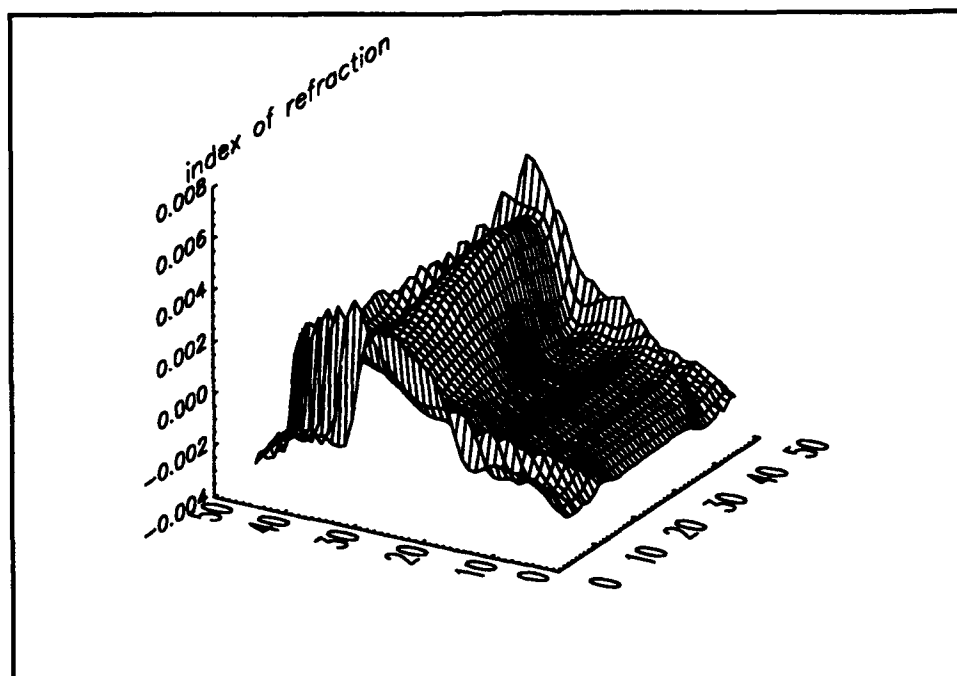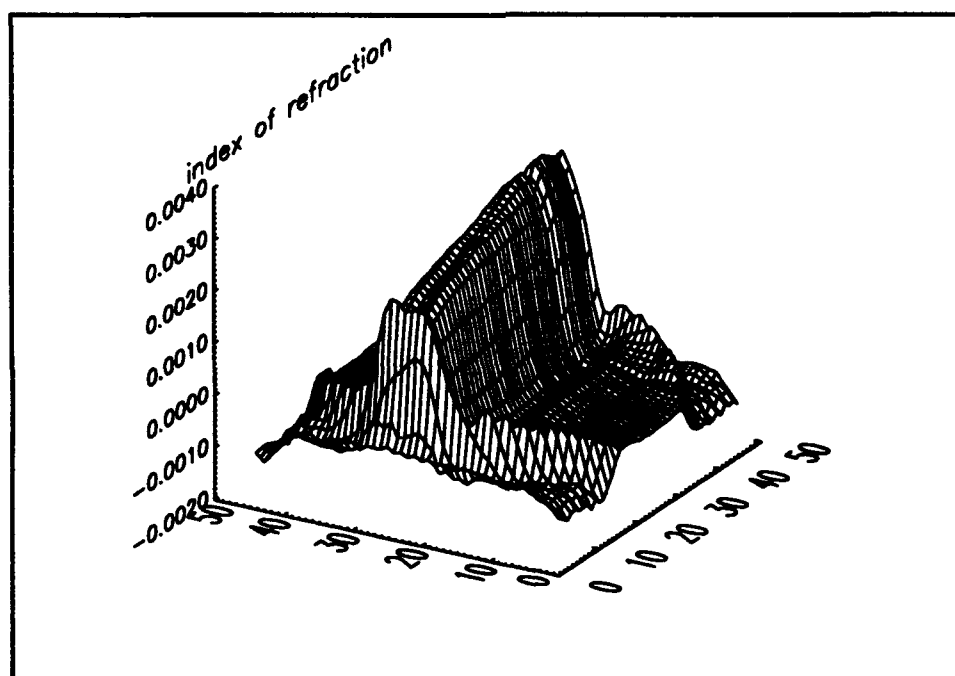

Figure 20. Plot of index of refraction variation, $2\pi\Delta n$, in the x-y plane at z=29, template #2.
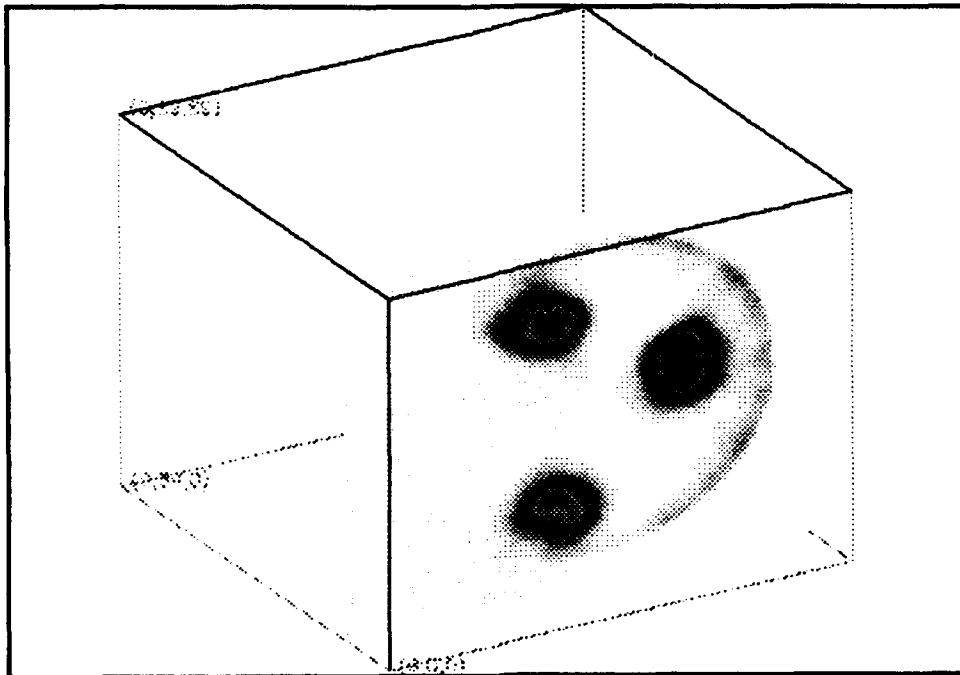
Figure 21. Cross-section of the reconstructed index of refraction plot for template #2 at Y=15.
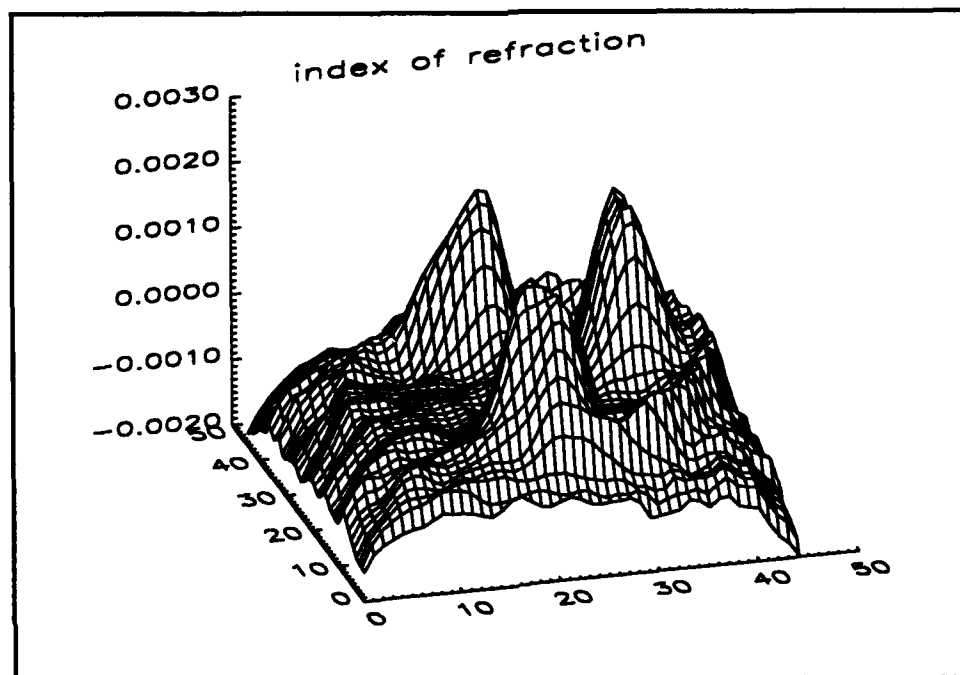

Figure 22. Plot of index of refraction variation, $2\pi\Delta n$, in the x-z plane at y=15, template #2.

35

The reconstruction for template #3 showed the expected characteristics in all three jets. Figure 23 shows a cross-section near the nozzle, along with a cross-section along the length of one of the jets. Figure 24 and 25 show the surface plots of the cross-sections in Figure 23. Figure 26 shows a cross-section away from the nozzle, with the surface plot in Figure 27. All three jets again contain the crescent notch aberration resulting from the circular aperture. In Figure 25 there is evidence of a notch across the jet of air. This notch is the result of bad pixels in the projection data. This bad area can be seen in several of the projections in the Appendix, particularly Figure A-3. Bad pixels usually result from insufficient light levels at the CCD cameras. This low light level was probably caused by a piece of dust on an optic or some similar aberration.

Figure 23. Cross-sections of the reconstructed index of refraction plot for template #3 at Y=75 and Z=21.

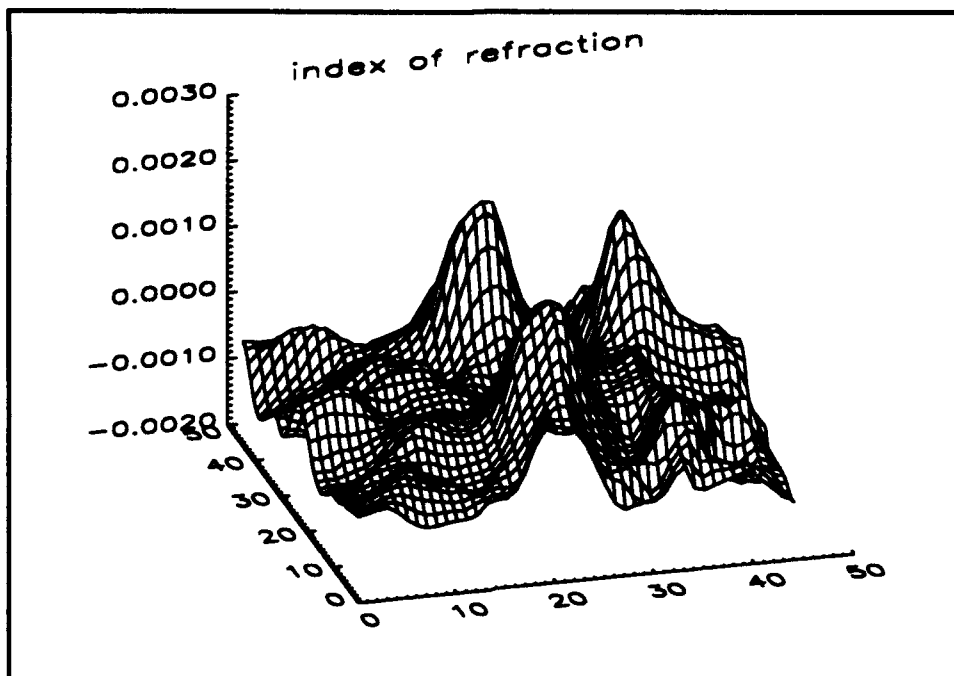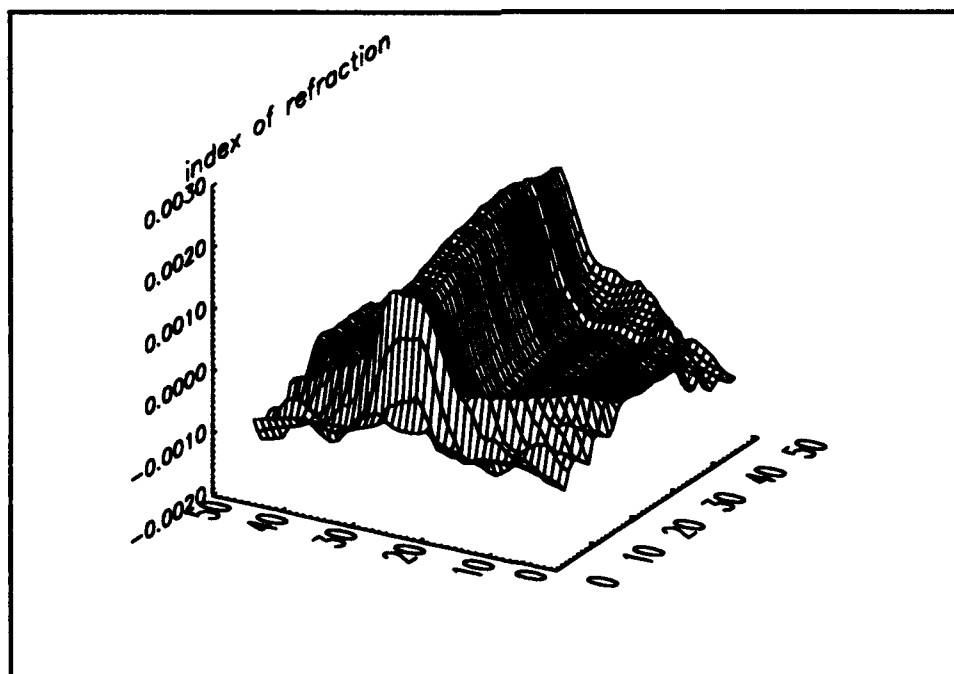**Figure 24.** Plot of index of refraction variation, $2\pi\Delta n$, in the x-z plane at y=75, template #3.

Figure 25. Plot of index of refraction variation, $2\pi\Delta n$, in the x-y plane at Z=21, template #3.

Figure 26. Cross-section of the reconstructed index of refraction plot for template #3 at Y=15.

Figure 27. Plot of index of refraction variation, $2\pi\Delta n$, in the x-z plane at y=15, template #3.

A reconstruction was performed for template #3 using only part of the available data. The projection data at every 30 degrees from 0 to 180 degrees was chosen. Therefore, the reconstruction was based on only seven angles, as opposed to the 19 angles used in the original reconstruction. The resulting reconstructed index of refraction plot matched the predicted outcome quite well. The sparse data set resulted in more artifacts, or noise within the reconstructed index of refraction than was seen with the full set of data. The increased noise is evident in the cross-section surface plots. Figure 28 shows a cross-section near the nozzle and a cross-section along the length of one of the jets. Figures 29 and 30 are the surface plots of the cross-sections in Figure 28. Figure 31 shows a cross-section further from the nozzle, with the corresponding surface plot in Figure 32.
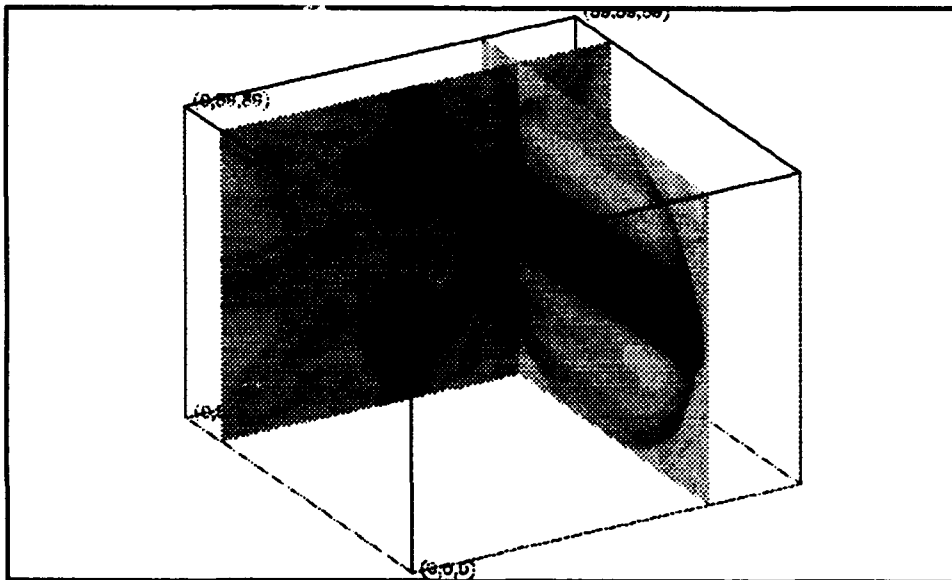
Figure 28. Reconstructed index of refraction plot for template #3 with a sparse data set. Cross-sections at Y=75 and Z=21.

Figure 29. Plot of index of refraction variation, $2\pi\Delta n$, in the x-z plane at Y=75. Template #3 with a sparse data set.

Figure 30. Plot of index of refraction variation, $2\pi\Delta n$, in the x-y plane at z=21. Template #3 with a sparse data set.

40
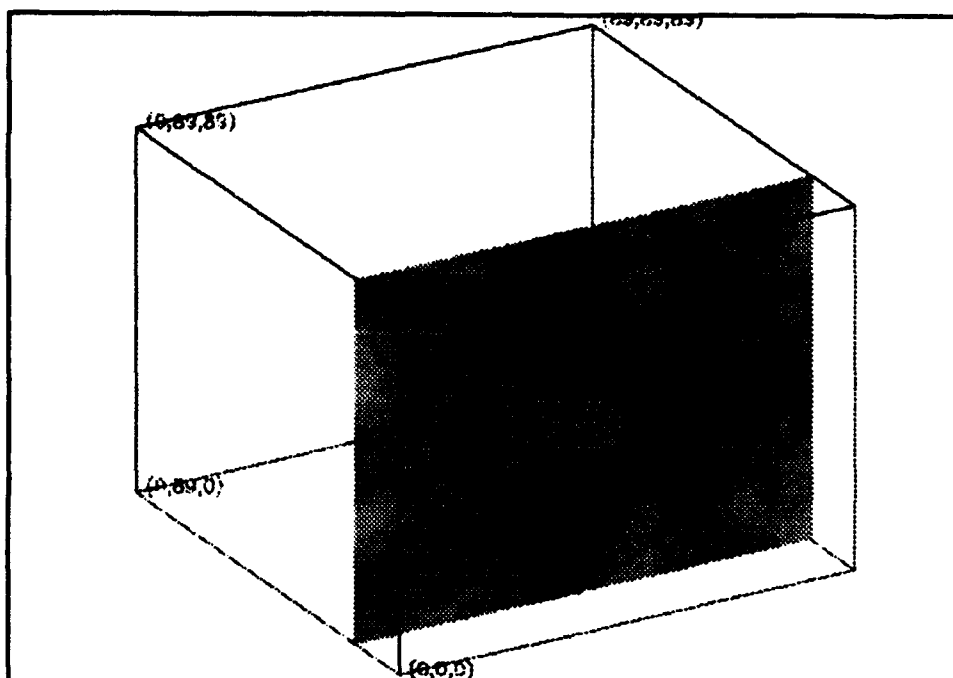
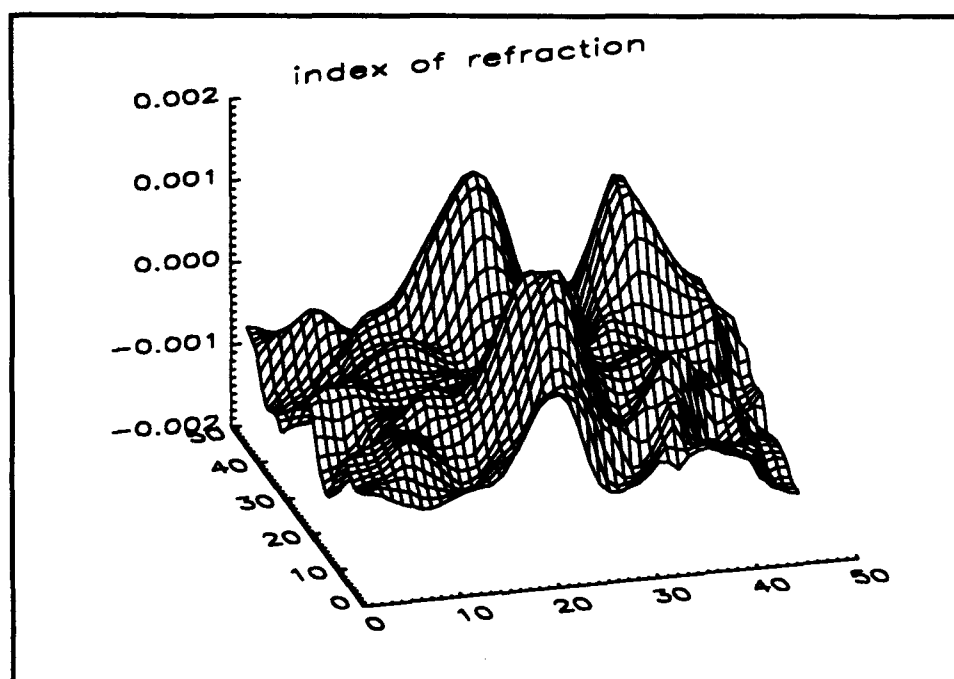**Figure 31.** Reconstructed index of refraction plot for template #3 with a sparse data set. Cross-section at Y=15.

Figure 32. Plot of index of refraction variation, $2\pi\Delta n$, in the x-z plane at y=15. Template #3 with a sparse data set.

41

V. Conclusions

The experiment demonstrated a unique approach to measuring the index of refraction of a turbulent field. Wave front sensor measurements were used as data for a tomographic reconstruction of the index of refraction field. A tomographic reconstruction is useful due to the fact that it provides cross sectional information of the turbulent flow. Therefore, we can observe any path through the turbulent flow and observe the index of refraction variation. Knowledge of the index of refraction variation permits the determination of the phase perturbation which will be induced in an optical wave propagating through the turbulent flow. Current techniques for reconstructing turbulence perform a line integral through the turbulent flow, providing the index of refraction information for only one optical path. The tomographic reconstruction is superior since it is capable of providing the index of refraction information for any path through the turbulent flow.

The experiment provided excellent results, as shown in the preceding chapter. The reconstruction for template #2 did not perform as well, but the aperture configuration was not optimum for the test being performed. The reconstruction for the index of refraction produced by templates #1 and #2 provided results exactly as expected. The only aberration in the reconstructions resulted from the effects of the aperture, as described in Section 4.1. The experiment accomplished the goals set forth and verified the feasibility of the tomographic technique for measuring turbulence structure.

5.1 Recommendations for future research

There is considerable follow on work which could be done in the area of tomographic reconstruction turbulent structure. The use of other wave front sensors, particularly a Hartmann sensor, for measuring the phase distortion could be examined. The Hartmann sensor may be able to provide data in a more timely manner. The actual number of projections needed to provide a reasonable reconstruction could also be examined in detail. As shown in Section 4.4, an acceptable reconstruction may be achieved with a relatively small number of projections. Reducing the number of projections not only decreases the data collection time, but it also decreases the computational time. Another way to speed up the reconstruction process is to examine the length of time over which the projection data must be gathered to provide the time averaged information. The 16 data frames used in the current experiment may be excessive. Fewer data frames would reduce the analysis time needed to calculate the phase maps significantly.

Another area which could be explored is the reconstruction algorithm which provides the best results. A multitude of reconstruction algorithms are available. An algorithm may be found which deals well with the specific parameters of the turbulence problem. Modifications of the various reconstruction algorithms could be experimented with to determine which technique provides the most accurate reconstruction of the index of refraction with the least available data.

A final area which needs to be looked at is the actual turbulence which we want to model. The nozzle system used for the current experimentation was suitable

for a verification of the technique, but does not treat the real world problem. A method of creating turbulence in the laboratory with structure resembling the structure seen in aero-optic turbulence is required. Testing could be done in a wind tunnel where a turbulent flow resembling aero-optic turbulence could be generated.

Appendix: Projection Data

The appendix contains a representative example of the projection data used in the tomographic reconstruction presented in Chapter 4. The projection data presented in the appendix corresponds to template #3. There are 19 wave front plots representing the data for the 19 angular views, zero to 180 degrees in 10 degree increments.
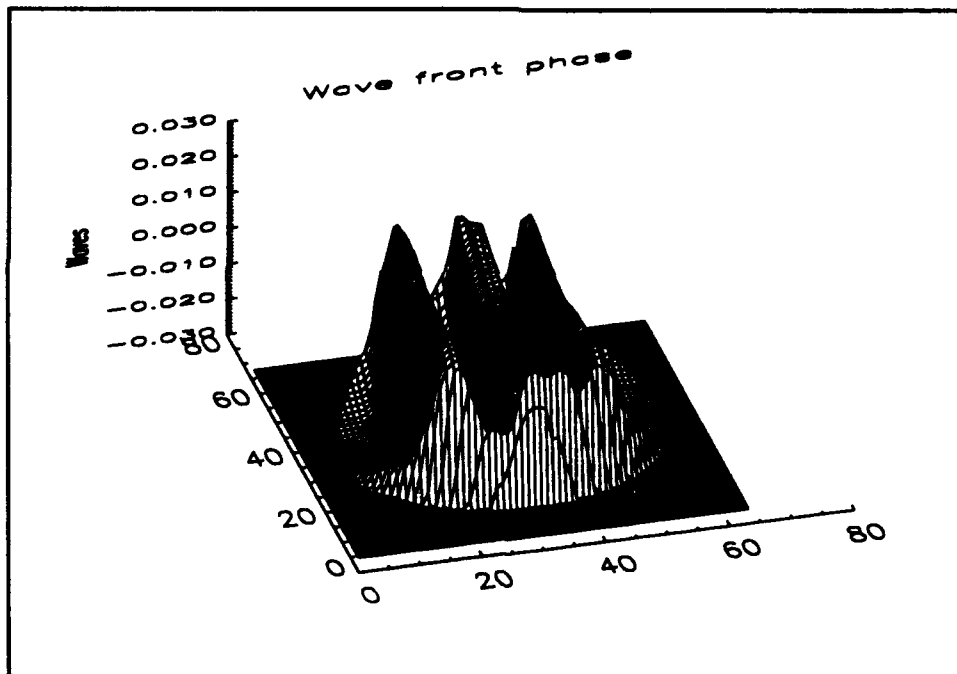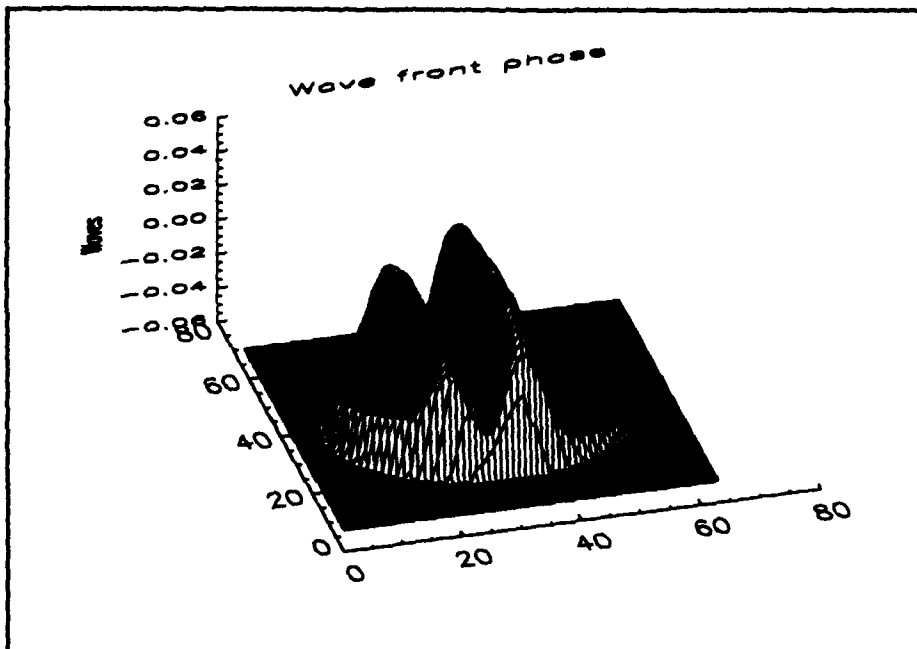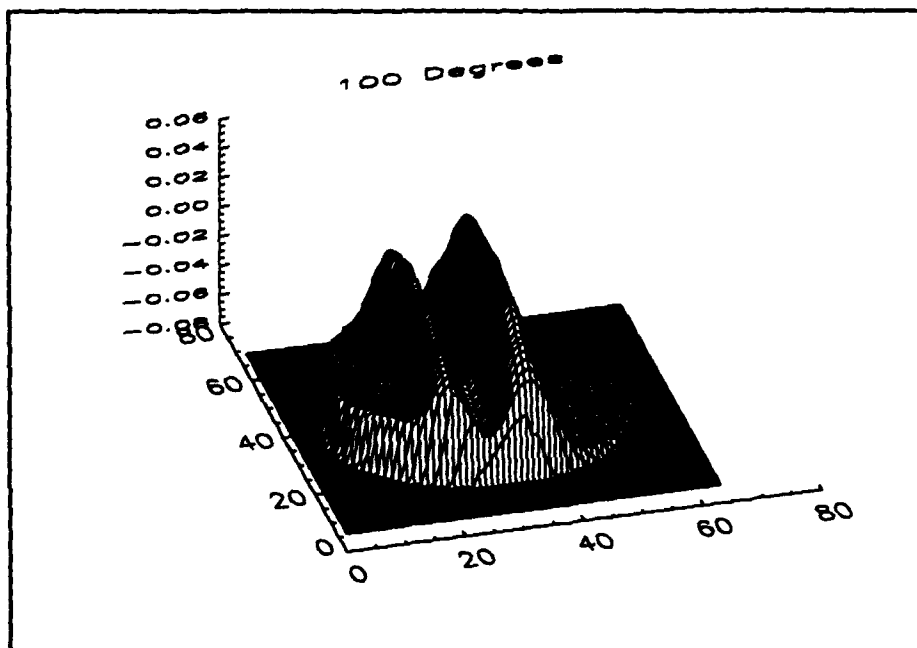

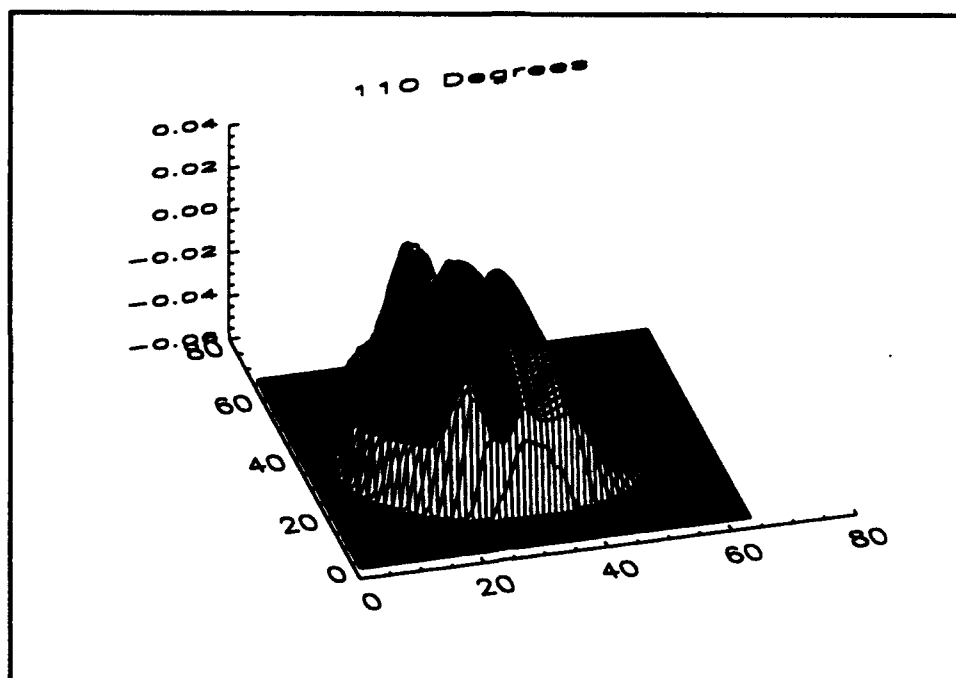**Figure A-1.** Projection data at 0 degrees.
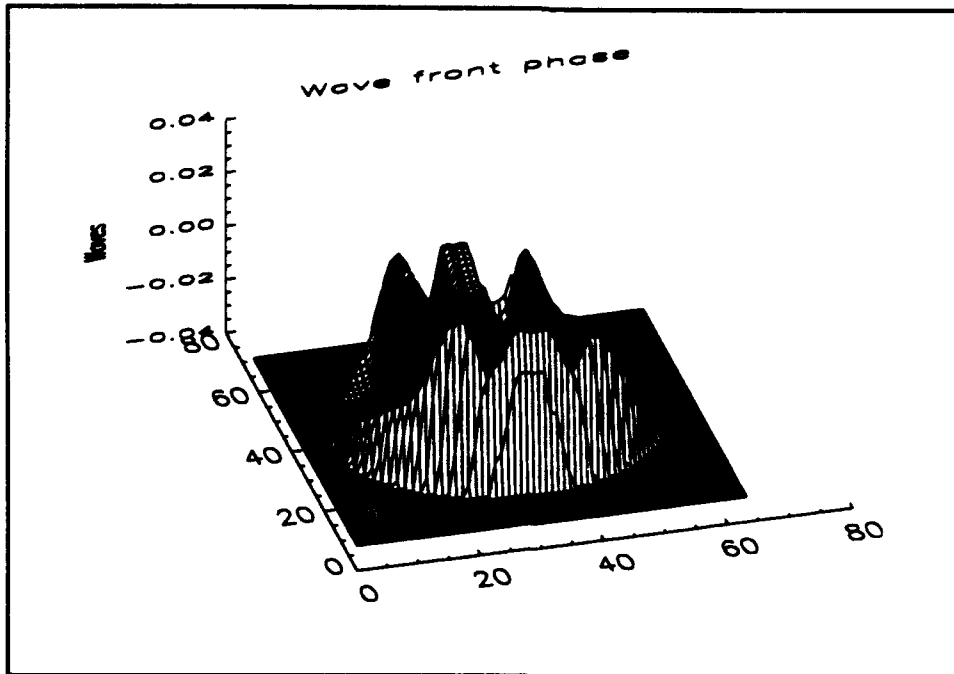
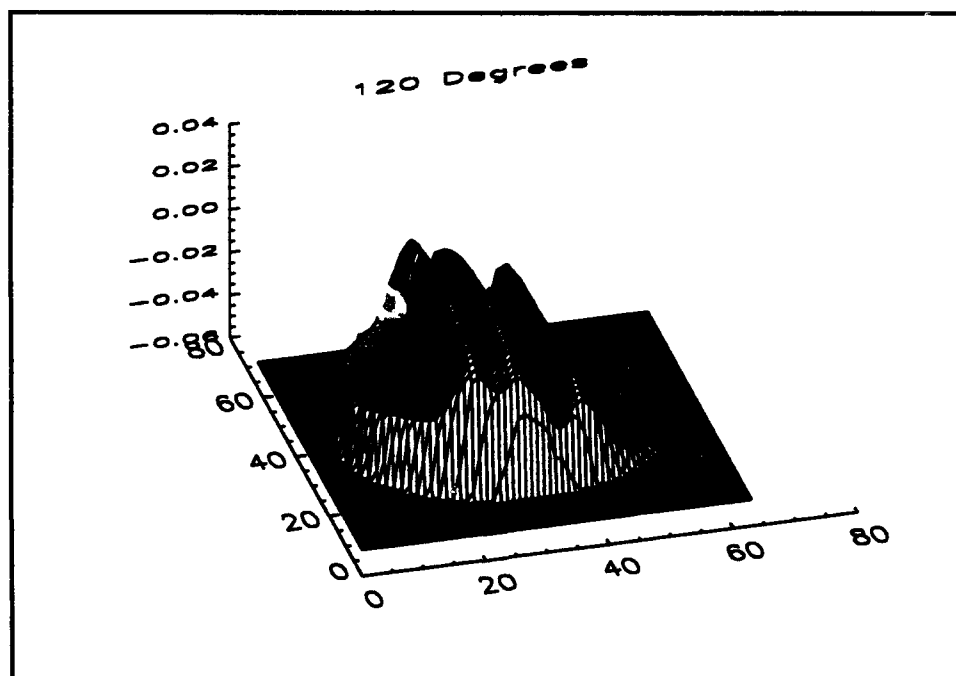**Figure A-2.** Projection data at 10 degrees.
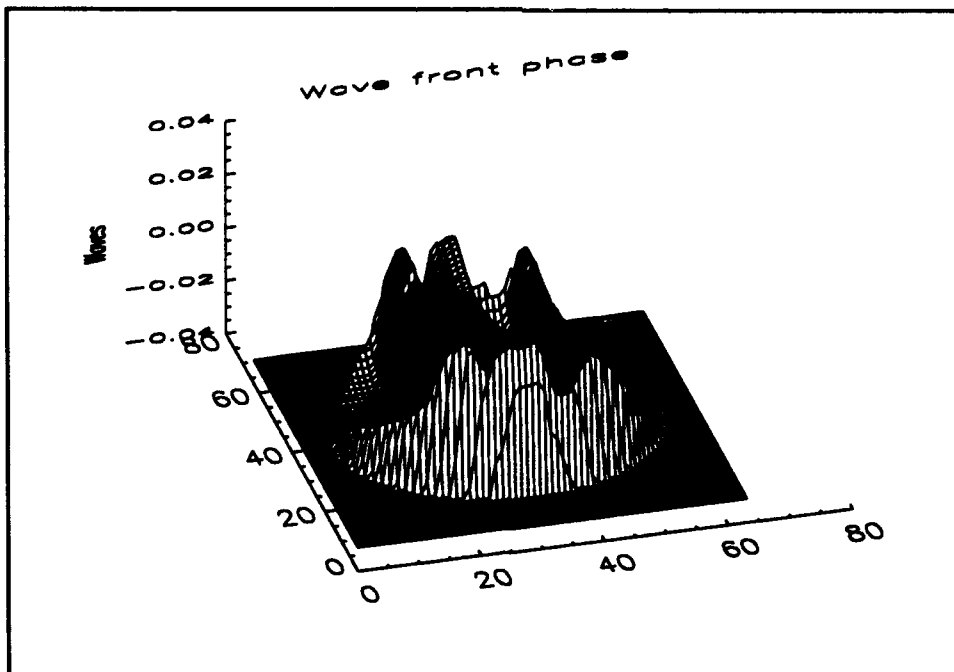
Figure A-3. Projection data at 20 degrees.
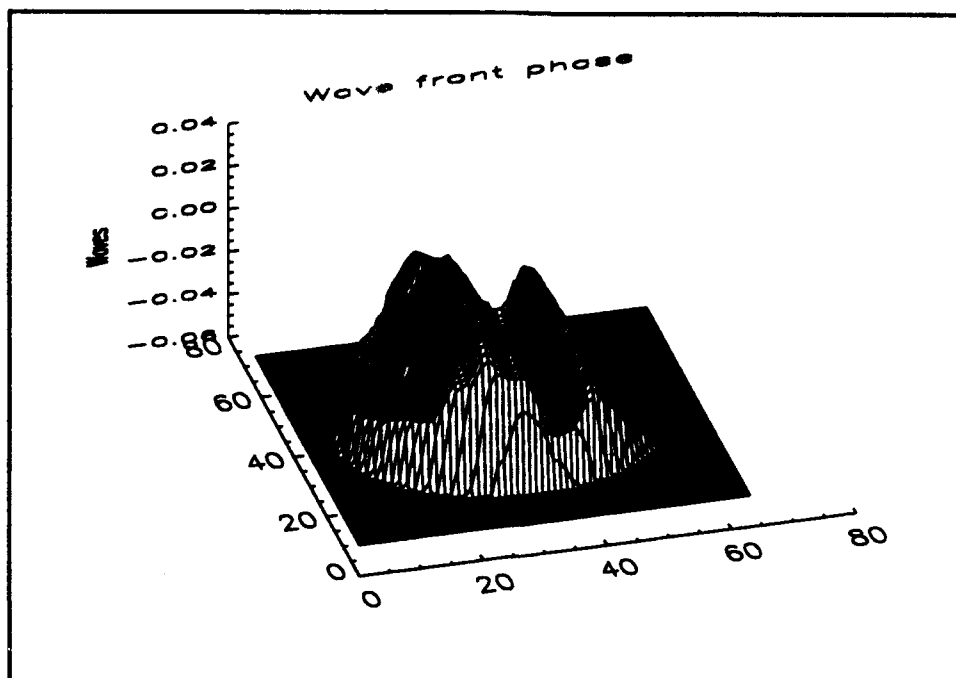
Figure A-4. Projection data at 30 degrees.
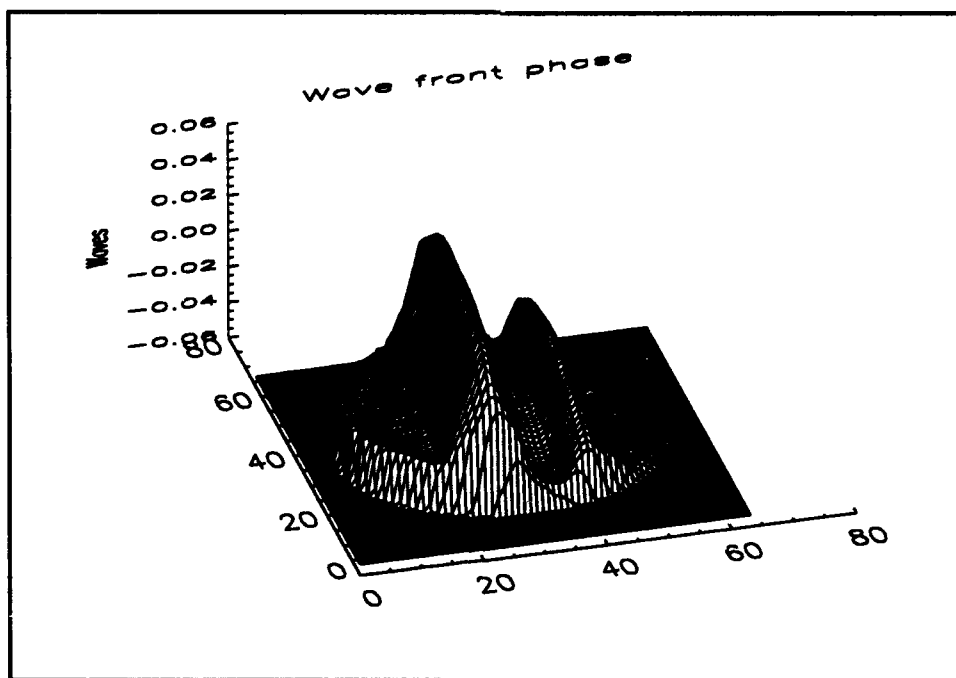
Figure A-5. Projection data at 40 degrees.
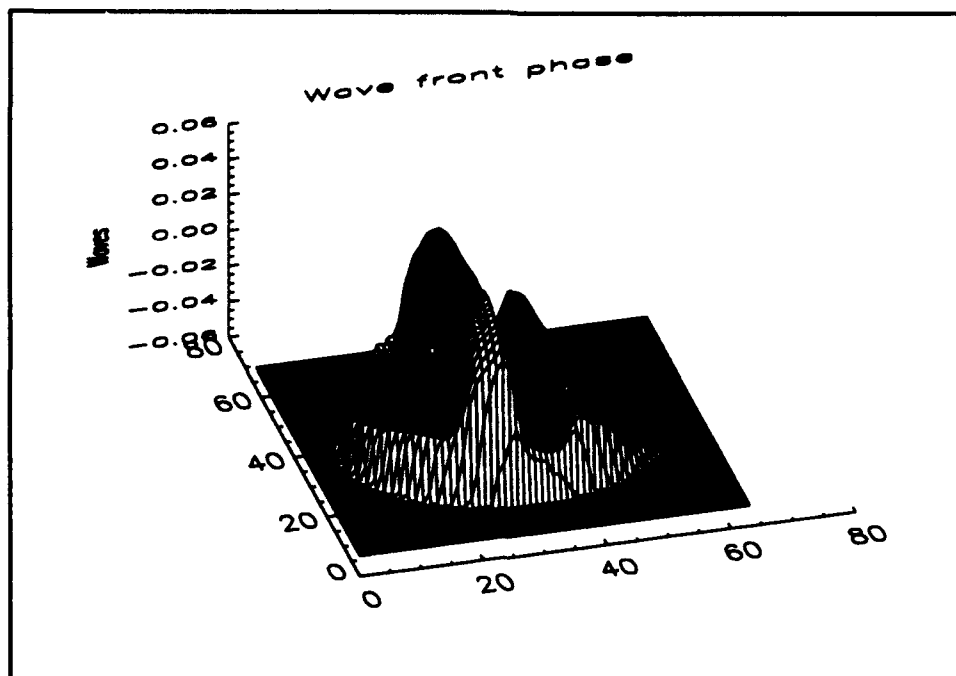
Figure A-6. Projection data at 50 degrees.
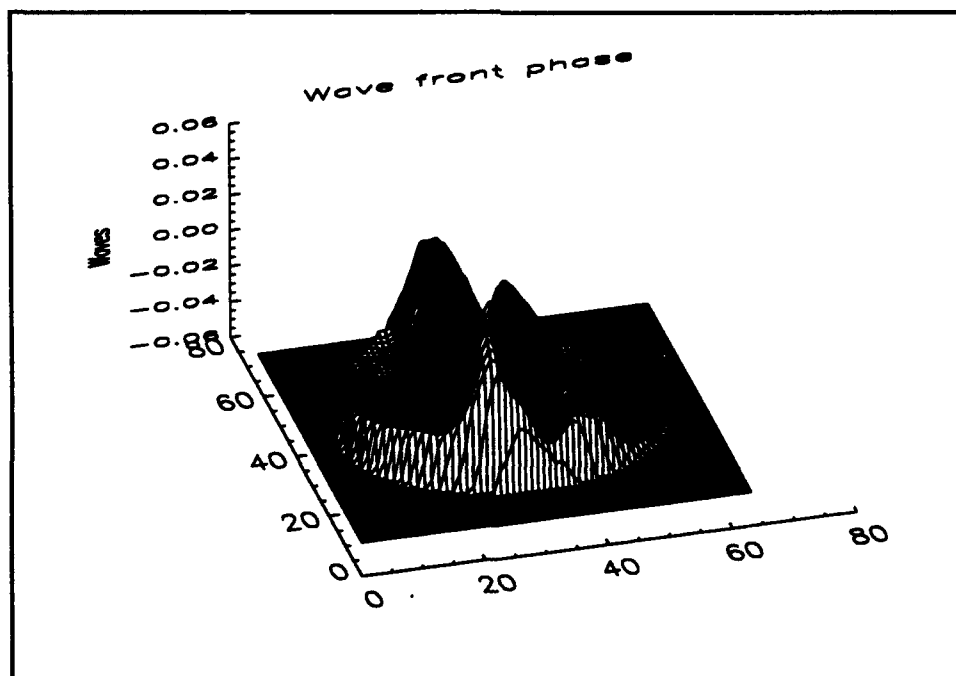
Figure A-7. Projection data at 60 degrees.

Wave front phase
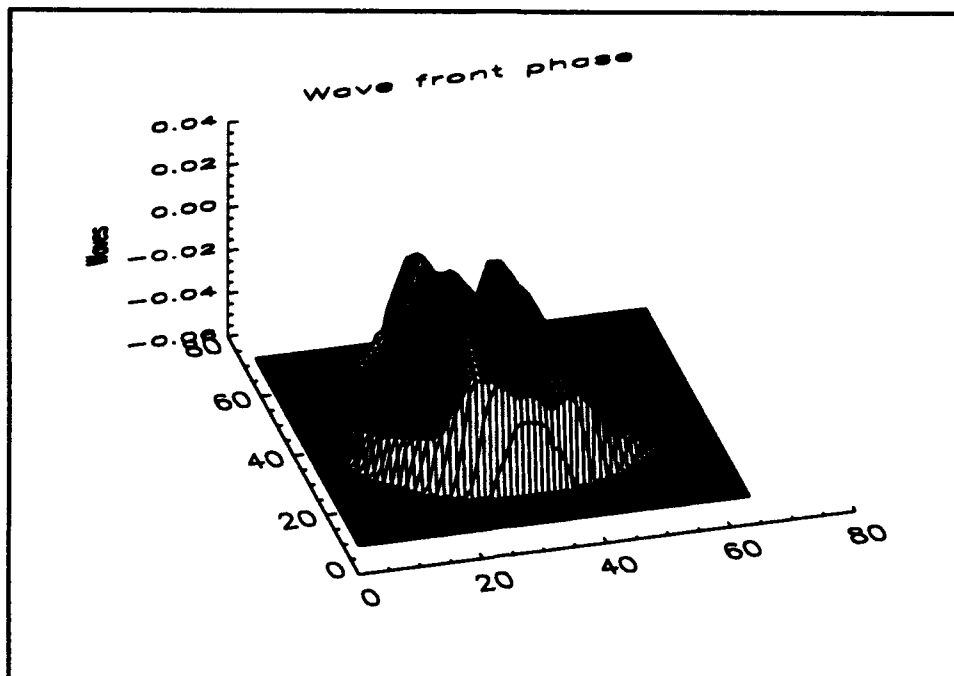
Figure A-8. Projection data at 70 degrees.

Wave front phase
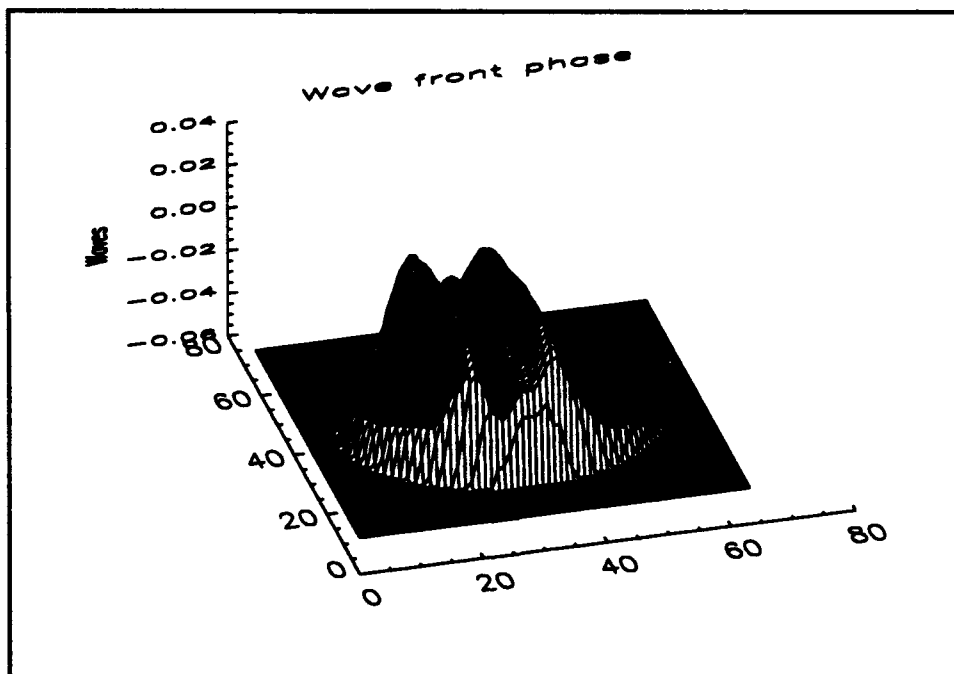
Figure A-9. Projection data at 80 degrees.

Figure A-10. Projection data at 90 degrees.

Figure A-11. Projection data at 100 degrees.

A-6

Figure A-12. Projection data at 110 degrees.

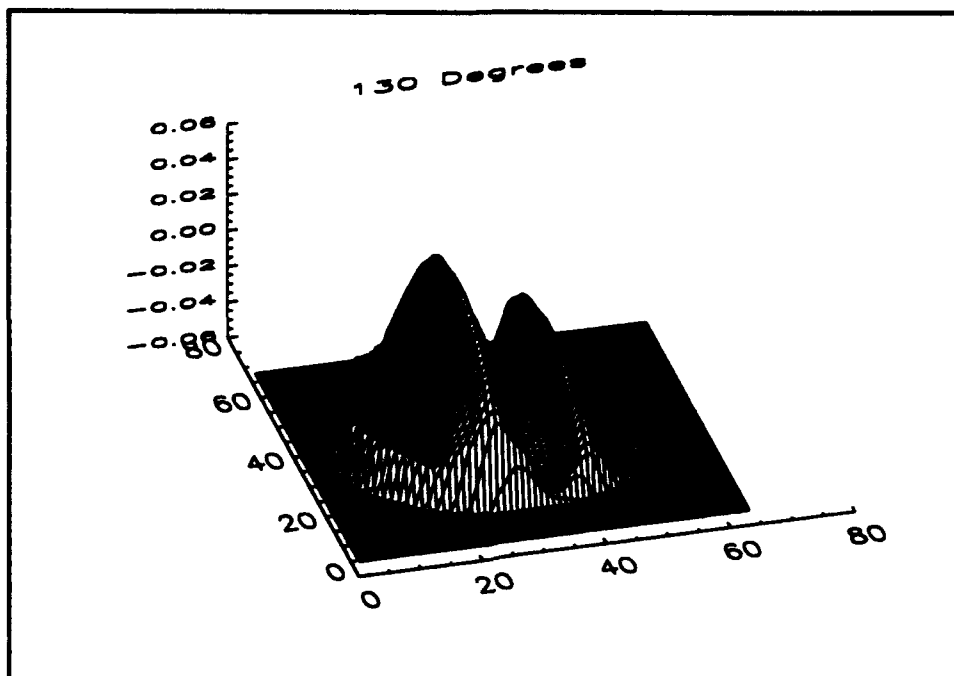**Figure A-13.** Projection data at 120 degrees.

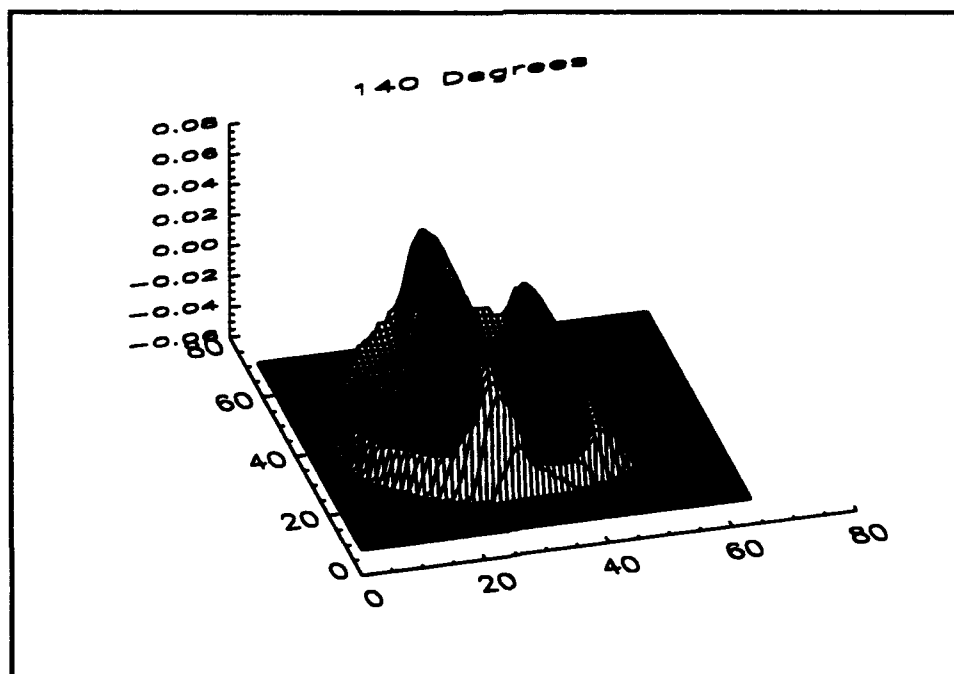**Figure A-14.** Projection data at 130 degrees.
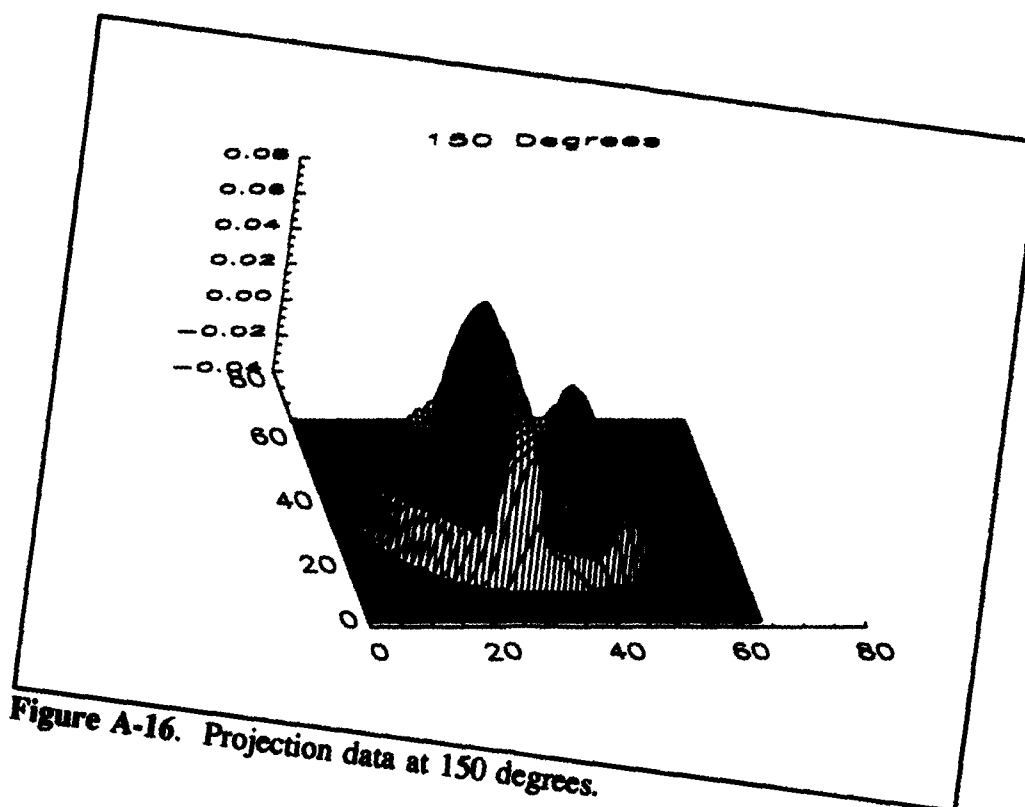

Figure A-15. Projection data at 140 degrees.
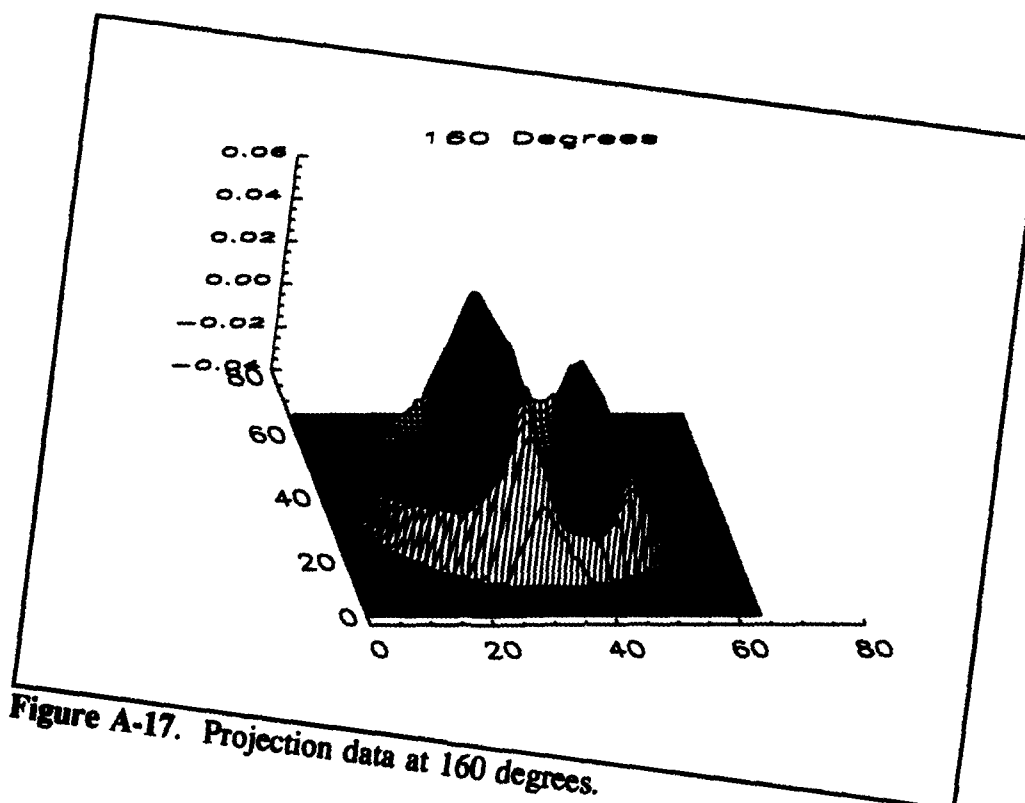
Figure A-16. Projection data at 150 degrees.

Figure A-17. Projection data at 160 degrees.
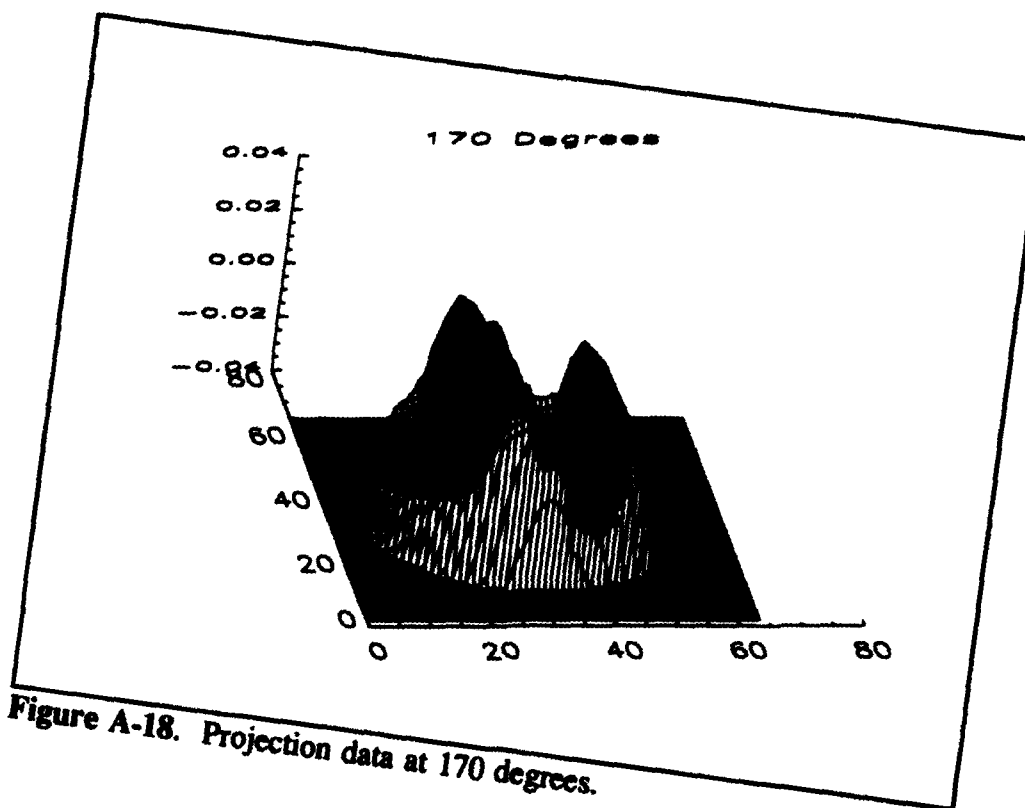
A-9

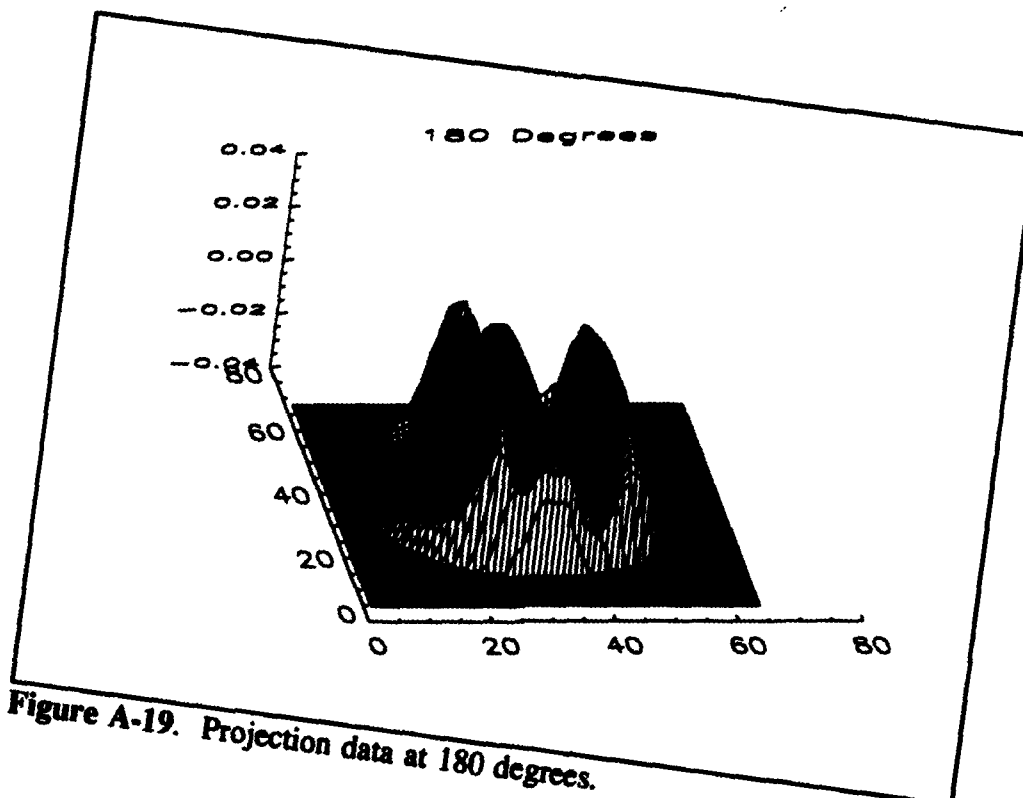**Figure A-18.** Projection data at 170 degrees.

Figure A-19. Projection data at 180 degrees.

A-10

Bibliography

1. Barret, Harrison H. and William Swindell. *Radiological Imaging*. New York: Academic Press, 1981.

2. Havener, George. "Optical Wave Front Variance: A Study on Analytic Models in Use Today, AIAA 92-0654." 30th Aerospace Sciences Meeting and Exhibit, January, 1992.

3. Hayner, D. A. and W. K. Jenkins. *Advances in Computer Vision and Image Processing, Vol. 1*. JAI Press, 1984.

4. Huesman, R. H. and others. *RECLBL Library Users Manual*. Lawrence Berkeley Laboratory, University of California, 1977.

5. Johnson, Robert L. *Numerical Simulation of Tomographic Reconstruction for the Study of Turbulence Using Wavefront Sensor Measurements*. MS thesis, AFIT/GAP/ENP/93D-4. Graduate School of Engineering, Air Force Institute of Technology (AU), Wright-Patterson AFB, OH, March 1993.

6. Magee, Eric P. *Characterization of Laboratory Generated Turbulence by Optical Phase Measurements*. MS thesis, AFIT/GEO/ENG/93M-03. School of Engineering, Air Force Institute of Technology (AU), Wright-Patterson AFB, OH, March 1993.

7. Sutton, George W. "Aero-optical Foundations and Applications," *AIAA Journal, Vol. 23, No. 10*: 1525-1537 (October 1958).

8. Tatarski, V. I. *Wave Propagation in a Turbulent Medium*. New York: Dover Publication, Inc., 1958.

9. Truman, C. Randall. "The Influence of Turbulent Structure on Optical Phase Distortion Through Turbulent Shear Flows, AIAA 92-2817." AIAA SDIO Annual Interceptor Technology Conference, May 1992.

10. Truman, C. Randall and Moon Joo Lee. "Effects of Organized Turbulence Structures on the Phase Distortion in a Coherent Optical Beam Propagating Through a Turbulent Shear Flow," *Physics of Fluids A, Vol. 2, No. 5*: 851-857 (May 1990).

11. Wissler, John B. and Anatol Roshko. "Transmission of Thin Light Beams Through Turbulent Mixing Layers, AIAA 92-0658." 30th Aerospace Sciences Meeting and Exhibit, January 1992.

Vita

Bryon L. Pedersen earned a Bachelor of Science degree in Electrical Engineering from South
Dakota State University in December of 1986. At the time of his graduation, he was
commissioned as a second lieutenant in the United States Air Force Reserve. He entered
active duty in October 1987, and was stationed at the 4950th Test Wing, Wright-Patterson
AFB, OH. While at the 4950th Test Wing he was involved with a multitude of flight test
programs ranging from radar jamming systems to IR sensor systems to optical data collection
systems. In June of 1992 he was enrolled in the Air Force Institute of Technology, Wright-
Patterson AFB, OH, where he pursued a Master of Science degree in Electrical Engineering,
specializing in Electro-Optics.

Permanent Address: 108 3rd Street

Arlington, SD 57212

REPORT DOCUMENTATION PAGE

1. AGENCY USE ONLY (Leave blank)	2. REPORT DATE December 1993	3. REPORT TYPE AND DATES COVERED Master's Thesis

4. TITLE AND SUBTITLE

EXPERIMENTAL VERIFICATION OF TOMOGRAPHIC RECONSTRUCTION OF TURBULENT AIR FLOW STRUCTURE USING OPTICAL WAVE FRONT MEASUREMENTS

5. FUNDING NUMBERS

6. AUTHOR(S)

Bryon L. Pedersen, Captain, USAF

7. PERFORMING ORGANIZATION NAME(S) AND ADDRESS(ES)

Air Force Institute of Technology, WPAFB OH 45433-6583

8. PERFORMING ORGANIZATION REPORT NUMBER

AFIT/GEO/ENG/93D-01

9. SPONSORING / MONITORING AGENCY NAME(S) AND ADDRESS(ES)

Captain John Wissler
PL/LIMI
Kirtland AFB, NM 87117-6008

10. SPONSORING / MONITORING AGENCY REPORT NUMBER

11. SUPPLEMENTARY NOTES

12a. DISTRIBUTION / AVAILABILITY STATEMENT

Approved for public release; distribution unlimited

12b. DISTRIBUTION CODE

13. ABSTRACT (Maximum 200 words)

The performance of an aircraft based optical system is degraded by aero-optic turbulence. The varying index of refraction within the turbulent field causes phase perturbation in an optical wave. In order to compensate for aero-optic turbulence effects, the nature of the turbulence must be understood. Large scale, organized structure within the turbulence has been found to contribute significantly to the overall phase perturbation caused by a turbulent field. A unique approach was devised to determine the turbulence structure using tomographic reconstruction techniques. Tomography provides an excellent means to determine the underlying structure within a turbulent field. The tomographic reconstruction produces a three-dimensional index of refraction plot of the turbulent field, revealing the structure within the turbulent field. An experiment was designed to determine the feasibility of the tomographic technique for reconstructing the turbulence structure. An optical wave was propagated through a turbulent field. A shearing interferometer was used to measure the wave front of the perturbed optical wave. The wave front phase map provided the projection data for a tomographic reconstruction of the index of refraction of the turbulent field. The experimental results verified the feasibility of the tomographic technique.

14. SUBJECT TERMS

Aero-optic turbulence, tomographic reconstruction, tomography

15. NUMBER OF PAGES
63

16. PRICE CODE

17. SECURITY CLASSIFICATION OF REPORT Unclassified	18. SECURITY CLASSIFICATION OF THIS PAGE Unclassified	19. SECURITY CLASSIFICATION OF ABSTRACT Unclassified	20. LIMITATION OF ABSTRACT UL